WIRELESS AND BATTERYLESS INSTANT VELOCITY SENSOR FOR CERTAIN DAILY MOTIONS

by

Burak Arıcıoğlu

B.S., Electrical and Electronics Engineering, Bogaziçi University, 2011

Submitted to the Institute for Graduate Studies in
Science and Engineering in partial fulfillment of
the requirements for the degree of
Master of Science

Graduate Program in Electrical and Electronics Engineering
Boğaziçi University

2014

WIRELESS AND BATTERYLESS INSTANT VELOCITY SENSOR FOR CERTAIN DAILY MOTIONS

APPROVED BY:

Assoc. Prof. Şenol Mutlu .....
(Thesis Supervisor)

Prof. Cem Ersoy .....

Assist. Prof. Ahmet Öncü .....

DATE OF APPROVAL: 18.07.2014

ACKNOWLEDGEMENTS

I would like to thank my thesis supervisor Assoc. Prof. Şenol Mutlu for his invaluable guidance and help during the every stage of the thesis project.

I would also like to thank my friend Emre İşeri for his valuable contributions.

This work is supported by Bogazici University Research Fund under Grant 7641.

ABSTRACT

WIRELESS AND BATTERYLESS INSTANT VELOCITY SENSOR FOR CERTAIN DAILY MOTIONS

The miniaturization studies in both integrated circuits (IC) and microelectromechanical systems (MEMS) have made it possible to have electronic systems that can operate with very low power. Sensors that are used for monitoring in the buildings, factories or military facilities and wireless sensor networks are examples of such systems. Most of these systems are powered up via batteries which may cause some problems such as replacement of the batteries or disposal of these batteries. Since these systems can operate with very low power, they can be powered up with miniature renewable energy sources. The energy sources that are used in such systems are commonly: solar, thermal, acoustical, mechanical and vibrational energy harvesting systems. Another main energy harvesting source is the ambient motion. It is possible to have a harvesting system, that utilizes human motion, which can power some small mobile equipment. In this thesis, a system is designed that harvest energy from human motion by electromagnetic induction to sense certain daily motions.

ÖZET

BAZI GÜNLÜK HAREKETLER IÇIN KABLOSUZ VE PILSIZ ANLIK HIZ SENSÖRÜ

Son yıllardaki elektronik entegrelerde ve mikro elektromekanik sistemlerdeki (MEMS) minyatürleştirme çalışmaları sayesinde bazı elektronik aletler ve sensörler çok düşük güç ile çalışabilmektedir. Bunlara örnek olarak; binalarda kullanılan sensörler, askeri amaçlı kullanılan sensörler, kablosuz sensör ağları gibi örnekler verilebilir. Bu sistemlerin enerjilerinin pil ile sağlanmasının bazı dezavantajları vardır. Bu dezavantajlardan bazıları: pillerin belli bir ömrü olması, pillerin içinde çevreye zararlı madde olmasıdır. Bu sistemlerın çalışması için gereken enerji düşük olduğundan, bu sistemlerde pillerin yerine minyatür çapta yenilenebilir enerji kaynaklarının kullanılmasına olanak sağlar. Genel olarak kullanılan enerji kayakları: güneş, termal, akustik ve mekaniktir ve son yıllarda da titreşim ile eneji hasatı yaygınlaşmıştır. Bu tez çalışmasında, bazı günlük haraketleri algılayabilen ve elektromanyetik indüksiyon yöntemi ile enerji hasat edebilen bir sensör tasarlanmıştır.

TABLE OF CONTENTS

LIST OF FIGURES

LIST OF TABLES

LIST OF SYMBOLS

A	Cross-sectional area of interest
A_{coil}	Cross-sectional area of the coil
A_{wire}	Cross-sectional area of the coil wire
B	Magnetic field
C	Capacitance
J_{b}	Volume current density
K_{b}	Surface current density
L	Inductance
l_{coil}	Length of the coil
L_{coil}	Inductance of the coil
l_{mag}	Length of the magnet
l_{wire}	Length of the wire of the coil
m	Magnetic dipole
M	Magnetization
N	The number of turns of the coil
Q	Quality factor
r	Distance
R	Resistance
r_{coil}	The radius of the coil
R_{coil}	The resistance of the coil
r_{mag}	The radius of the magnet
r_{wire}	The radius of the coil of the wire
S	Surface area
v	Velocity
V_{c}	Voltage of the capacitor
α	Attenuation coefficient
ε	Electromotive forcel

ρ_{wire}	The resistivity of the wire
ϕ	The magnetic flux
μ_0	The permeability of the air
ω_0	Natural resonance frequency
ω_{d}	Damped natural frequency
ζ	The damping factor

LIST OF ACRONYMS/ABBREVIATIONS

2D	Two-dimensional
AC	Alternative current
ADC	Anolog to digitalconverter
IC	Integrated circuit
MEMS	Microelectromechanical systems
MOSFET	Metal oxide semiconductor field effect transistor
RC	Resistance capacitance circuit
RF	Radio frequency
RLC	Resistance, inductance and capacitance circuit

1. INTRODUCTION

Thanks to the miniaturization studies in the integrated circuits (IC) and micro electromechanical systems (MEMS) in the recent years, some sensor systems can operate with very low power and the power consumption of these systems has been reduced from m Watts to μ Watts [1]. Some examples of these systems are sensors which are used in buildings, military purpose sensors and wireless sensor networks and etc. [1–4]. Supplying power to such systems through batteries presents some disadvantages. Some of these disadvantages are large battery size, limited lifetime of the batteries, batteries contain hazardous material to environment and sometimes these batteries can be hard to replace [4]. Due to these system can function with low power, batteries can be replaced with miniature renewable energy sources. Some examples of renewable energy resources are solar, thermal, acoustic and mechanical energy. In the recent years, energy harvesting from vibration has become widespread [2]. There are more than one method for energy harvesting from vibration and these are electrostatic (capacitive), piezoelectric and electromagnetic induction [5].

The vibrational energy harvester systems are usually resonance systems [6–8] and for maximum efficiency, the Eigen frequency of the converter should be equal to the vibration frequency. Thus, the efficiency of the vibrational energy harvester systems if the frequency of the vibration is known and does not change, will be high. To harvest energy from non-resonant vibrations, some techniques are developed such as energy scavenging from vibrations via electromagnetic induction [9].

Another energy harvesting method via electromagnetic induction is energy harvesting from the nonlinear oscillations of magnetic levitation [10]. In this method, two magnets are fixed at the two ends of a tube and the third magnet is placed inside the tube. The magnets are placed in such a manner that both the two magnets at the ends of the tube repel the magnet in the middle [10].

Table 1.1. Comparison of energy harvesting techniques from vibration [11].

	Variable Capacitance	Piezo Material	Magnetic Induction
Power generation	μW	μW-W	mW-kW
Vibration amplitude	μm	μm	mm-cm
Driving frequency	Any range	Tens of Herz	Any range
Ease of system design	Difficult	Easy	Easy
Cost	High	High	Modest
Lifetime	Low	High	High

In this thesis, the energy harvesting will be done via electromagnetic induction, a magnet passes through a coil.

Most of the source for the energy harvester system is the ambient motion [12] and our every day motion, normally, get wasted and remain unused most of the time [13]. A system can be designed to utilize the human motion to scavenge energy.

In this work, electromagnetic induction energy harvester system, that utilizes human motion to harvest energy and characterize the motion from that energy, is designed.

The instant motion sensor that designed is shown in Figure 1.1. The working principles of the sensor are:

- The utilizing human motion to make magnet pass through the coil
- The magnet passing through the coil induces voltage to the coil
- Storage of the induced voltage to power up the sensor circuit
- Sensing the instant motion from stored energy
- Sending the motion data wirelessly

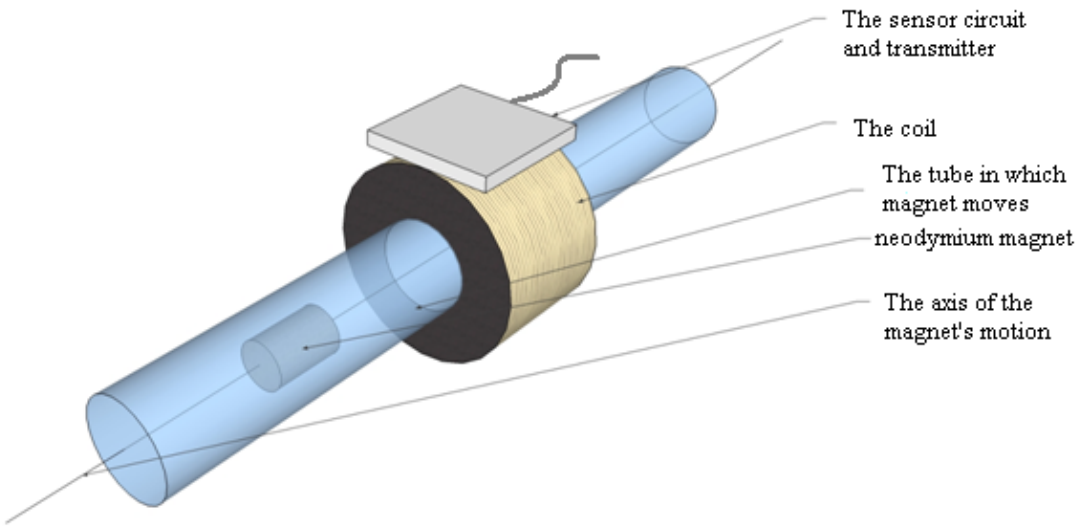

Figure 1.1. The proposed system for the instant motion sensor.

1.1. Transceiver Module STM 300

The STM 300 is one of the scavenger transceiver module of Enocean Company [14]. The STM 300 module is an extremely power saving RF transmitter module that enables the realization of wireless and maintenance free sensors and actuators such as room operating panels, motion sensors or valve actuators for heating control.

1.1.1. Features of STM 300 with built-in firmware

- 3 A/D converter inputs
- 4 digital inputs
- Configurable wake-up and transmission cycle
- Wake-up via Wake pins
- Voltage limiter
- Threshold detector
- Application notes for calculation of energy budgets and management of external energy storages

and it is possible to write custom firmware for the module.

2. THEORY

2.1. Electromagnetic Induction when a bar magnet passes through a coil

In this section analysis of electromagnetic induction when a bar magnet passes through a coil is made.

2.1.1. Magnetic Field of a Bar Magnet

The magnetic field source of a bar magnet comes directly from electron spins and orbital states [15]. For a uniformly magnetized cylinder, e.g. a bar magnet, the magnetization $\mathbf{M(x)}$, the dipole moment density, is constant, $\mathbf{M} = \mathbf{M}_0\hat{\mathbf{k}}$. Since $\mathbf{J}_b = \mathbf{V} \times \mathbf{M} = 0$ for uniform magnetization, there is no volume current. The surface current is again zero on the flat surfaces, $z = -l_{mag}/2$ and $z = l_{mag}/2$ where l_{mag} is the length of the magnet. There is bound surface current on the curved surface $r = r_{mag}$ where r_{mag} is the radius of the magnet, because there $\mathbf{K}_b = \mathbf{M} \times \hat{\mathbf{r}} = \mathbf{M}_0\hat{\phi}$ [15].

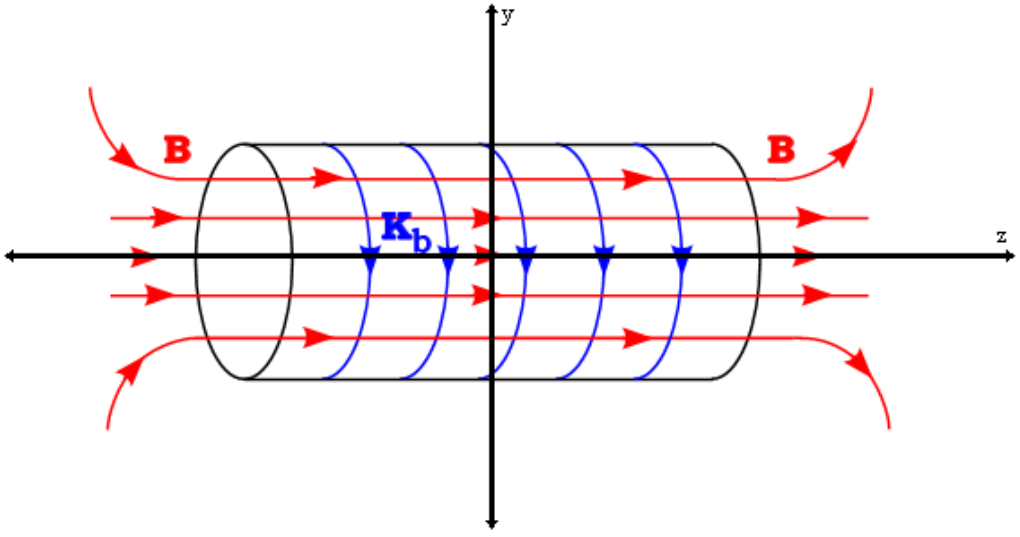

Figure 2.1. Illustration of the surface current $\mathbf{K}_b$ which produces magnetic field. [16].

Magnetic field of the bar magnet along the z-axis can be calculated as:

$$\mathbf{B}\,(0,0,z)\;=\;\frac{\mu_0 M_0}{2}\,(\frac{z\;+\;l_{\mathrm{mag}}/2}{\sqrt{{r_{\mathrm{mag}}}^2\;+\;(\,z\;+\;l_{\mathrm{mag}}/2\,)^2}}\;-\frac{z\;-\;l_{\mathrm{mag}}/2}{\sqrt{{r_{\mathrm{mag}}}^2\;+\;(\,z\;-\;l_{\mathrm{mag}}/2\,)^2}})\quad(2.1)$$

then, the magnetic field at the center of the magnet is:

$$\mathbf{B}\,(0,0,0)\;=\mu_0 M_0\,(\frac{l_{\mathrm{mag}}/2}{\sqrt{{r_{\mathrm{mag}}}^2\;+\;{l_{\mathrm{mag}}/2}^{\,2}}}\,)\qquad(2.2)$$

and the magnetic field at the end of the magnet:

$$\mathbf{B}\,(0,0,l_{\mathrm{mag}}/2)\;=\;\mathbf{B}\,(0,0,-l_{\mathrm{mag}}/2)\;=\;\frac{\mu_0 M_0}{2}\,(\frac{l_{\mathrm{mag}}}{\sqrt{{r_{\mathrm{mag}}}^2\;+\;{l_{\mathrm{mag}}}^{\,2}}}\,)\qquad(2.3)$$

where $\mathbf{M}_0$ is the dipole moment density.

2.1.2. Calculation of the Magnetic Flux at the Coil

Equation 2.1 is only valid for magnetic field along the z-axis. The magnetic field that is produced by the bar magnet at any point when the magnet is oriented along the polar axis can be calculated as [17]:

$$\mathbf{B}\;=\;\frac{\mu_0}{4\pi}\,\frac{m}{r^3}\,(2\cos\theta\,\hat{\mathbf{r}}\;+\;\sin\theta\,\hat{\theta}\,)\qquad(2.4)$$

where $m = \mathbf{M}_0 \pi {r_{\mathrm{mag}}}^2 l_{\mathrm{mag}}$, the magnetic dipole.

In Figure 2.2, a magnet with dipole moment m is passing through a coil is shown. The center of the magnet is aligned with the origin of the polar axis. The magnetic flux through the coil can be calculated by using the surface the spherical cap bounded by the coil as shown in Figure 2.2. The magnetic flux through the area element is:

$$\mathbf{B}.d\mathbf{A}\;=\;(\,\frac{\mu_0\,m}{4\pi r^3}\,2\cos\theta\,)\,r^2\;\sin\theta\,d\theta\,d\phi\qquad(2.5)$$

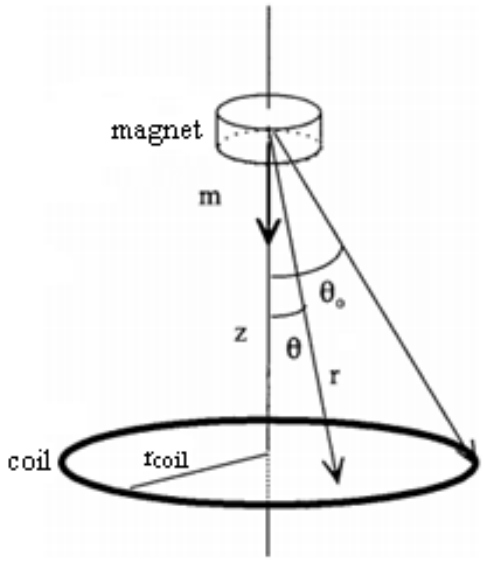

Figure 2.2. The model that is used for calculating the induced voltage at the coil [17].

Then the flux is the integral of Equation 2.5:

$$\phi = \int \mathbf{B}.d\mathbf{A} = \left(\frac{\mu_0 m N}{2r} \sin^2\theta_0 \right) \tag{2.6}$$

here N is the number of the turn of the coil, θ_0 is the angle from coil axis to coil and $\sin\theta_0 = r_{\text{coil}}/r$ and $r = \sqrt{{r_{\text{coil}}}^2 + z^2}$. Thus Equation 2.6 can be expressed as a function of z:

$$\phi = \frac{\mu_0 m N}{2} \frac{{r_{\text{coil}}}^2}{({r_{\text{coil}}}^2 + z^2)^{3/2}} \tag{2.7}$$

2.1.3. The calculation of the Induced Voltage at the Coil

Electromotor force (emf) which is created by electromagnetic induction at a coil can be calculated with Faraday's Law:

$$\varepsilon = -N \frac{d\phi}{dt} \tag{2.8}$$

$$\phi = \int\int_S B.dS \tag{2.9}$$

where: $\varepsilon =$ Electromotor force (emf), $N =$ number of turns of the coil, $\phi =$ Magnetic flux, $B =$ Magnetic field, $S =$ Surface area. As it seen in Equation 2.8 the magnitude of the induced emf is proportional the number of turns of the coil (N), and the change of rate of the magnetic flux.

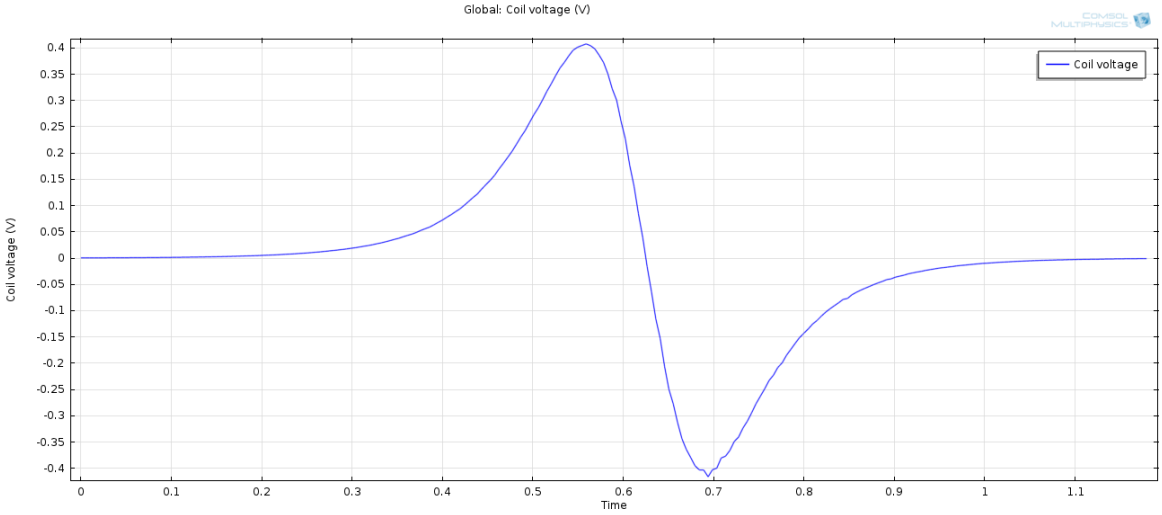

Figure 2.3. The characteristic shape of the induced voltage at the coil.

Equation 2.8 can be rearranged as:

$$\varepsilon = -N\frac{d\phi}{dt} = -N\frac{d\phi}{dz}\frac{dz}{dt} = -N\frac{d\phi}{dz}v \tag{2.10}$$

where v is the velocity of the magnet. If we substitute the flux in equation 2.7 into equation 2.10 then we get:

$$\varepsilon = \frac{3\mu_0 mNr_{\text{coil}}^2}{2}\frac{zv}{(r_{\text{coil}}^2 + z^2)^{5/2}} \tag{2.11}$$

If we take the derivative of the emf and solve the resulting equation, we can find for

which values of z the emf reach extreme points. The derivative of Equation 2.11 is:

$$\varepsilon^{'}(z) = \frac{3\mu_0 m N r_{\text{coil}}^2 v}{2} \frac{r_{\text{coil}}^2 - 4z^2}{(r_{\text{coil}}^2 + z^2)^{7/2}} \tag{2.12}$$

$\varepsilon^{'}$ is equal to zero when $z = \pm r_{\text{coil}}/2$. The extreme values of the induced emf is

$$\varepsilon_{e\pm} = \pm \frac{24\mu_0 m N v}{5^{5/2} r_{\text{coil}}^2} \tag{2.13}$$

As it is seen equation 2.13 the extreme values of the induced emf is proportional to the instant speed of magnet since the only variable in Equation 2.13 which is not constant is v the velocity of the magnet. Thus the instant speed of the magnet can be calculated as:

$$v = \frac{|\varepsilon_{e\pm}| \, 5^{5/2} r_{\text{coil}}^2}{24\mu_0 m N} \tag{2.14}$$

2.1.4. Calculation of Coil Inductance and Resistance

The inductance of the coil depends on the square of the number of turns of the coil (N), the length of the coil (l_{coil}) and the cross-sectional area of the coil ($A_{\text{coil}} = \pi {r_{\text{coil}}}^2$):

$$L_{\text{coil}} = \frac{\mu_0 N^2 A_{\text{coil}}}{l_{\text{coil}}} \tag{2.15}$$

The resistance of the coil depends on the resistivity, the length and the cross-sectional area of the wire. The length of the wire is also depends on the diameter of the coil ($2r_{\text{coil}}$) and the number of turns of the coil (N):

$$l_{\text{wire}} = \frac{\mu_0 N^2 A_{\text{coil}}}{l_{\text{coil}}} \tag{2.16}$$

and

$$R_{\text{coil}} = \frac{\rho_{\text{wire}} l_{\text{wire}}}{A_{\text{wire}}} = \frac{2\rho_{\text{wire}} r_{\text{coil}} N}{r_{\text{wire}}^2} \tag{2.17}$$

2.2. A rectifier and peak detector circuit for the energy harvesting system design

Since the characteristic shape of the induced voltage at the coil, when a magnet passes through it, is like a single-shot sinusoidal as in Figure 2.3, the induced voltage should be rectified. Since we want both to harvest the energy generated from the coil and the peak voltage value of the induced voltage to predict the velocity of the magnet, we need also a peak detector circuit. In Figure 2.4 simple circuit for the batteryless and wireless motion sensor is shown.

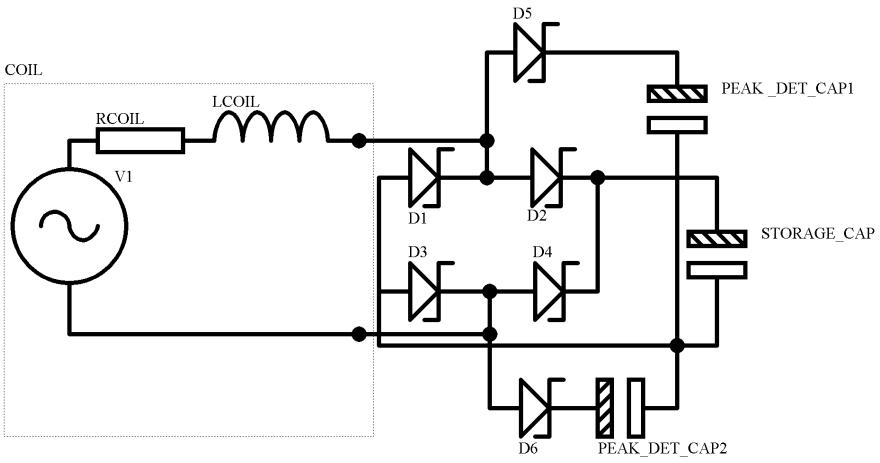

Figure 2.4. Basic schematic for energy harvesting system.

In Figure 2.4 D1, D2 , D3 and D4 diodes form bridge rectifier and most of the harvested energy will be stored in the storage capacitor. The diode D5 and the positive peak capacitor are used for detecting and storing the positive peak. The diode D6 and the negative peak capacitor are used for detecting and storing the negative peak. Both the positive and negative peak detectors are, in fact, a half wave rectifier, thus the

voltage at the both capacitors are positive.

2.3. A Simple RLC Analysis to Determine the Value of the Storage Capacitor

All the three circuit components resistor, inductor and capacitor are in series with the source. For simplicity, the source is a ramp function for both calculation and simulation. The governing differential equation for this RLC circuit:

$$\frac{d^2V_c(t)}{dt^2} + \frac{R}{L}\frac{dV_c(t)}{dt} + \frac{1}{LC}V_c(t) = \frac{1}{LC}r(t) \tag{2.18}$$

where R and L are the resistance and inductance of the coil, respectively, C is the storage capacitor and V_c indicates the voltage across the capacitor. Both the resistance and inductance values are function of the parameters of the coil. Some important parameters for series RLC circuit:

$$\alpha = \frac{R}{2L} \tag{2.19}$$

$$\omega_0 = \sqrt{\frac{1}{LC}} \tag{2.20}$$

$$\zeta = \frac{R}{2}\sqrt{\frac{C}{L}} \tag{2.21}$$

where α is the attenuation coefficient, ω_0 is the natural frequency of the circuit and ζ is the damping factor.

For the given coil parameters in Section 3.2 the calculated value of the inductance of the coil by using Equation 2.15, $L_{\text{coil}} = 2.2\ H$ and the calculated value of the resistance of the coil by using Equation 2.17, $R_{\text{coil}} = 1800\ ohms$. The input signal is $5tu(5-t)$. The initial conditions are zero, $V_c(0) = 0$ and $V_c{}'(0) = 0$.

2.3.1. Critically-damped Response

For the systems response to be critically damped the damping factor should be equal to one. If the damping factor $\zeta = \frac{R}{2}\sqrt{\frac{C}{L}} = 1$, then the value of the capacitor $C = 2.716\,\mu\text{F}$. The attenuation coefficient $\alpha = 414$ for the given R and L values. Homogenous response of the system:

$$V_{\text{CH}}(t) = Ate^{-\alpha t} + Be^{-\alpha t} \tag{2.22}$$

and the particular response of the system:

$$V_{\text{CP}}(t) = r(t) + D \tag{2.23}$$

The value of D can be calculated if we substitute the particular response in Equation 2.23 $V_{\text{CP}}(t)$ into equation 2.18, then $D = -\ 4.8877$. The response of the voltage across the capacitor becomes, $V_{\text{c}}(t) = Ate^{-414t} + Be^{-414t} + 1000t - 4.8877$. The values of A and B can be calculated by applying the initial conditions.

$$V_{\text{c}}(t) = 1000te^{-414t} + 4.8877e^{-414t} + 1000t - 4.8877 \tag{2.24}$$

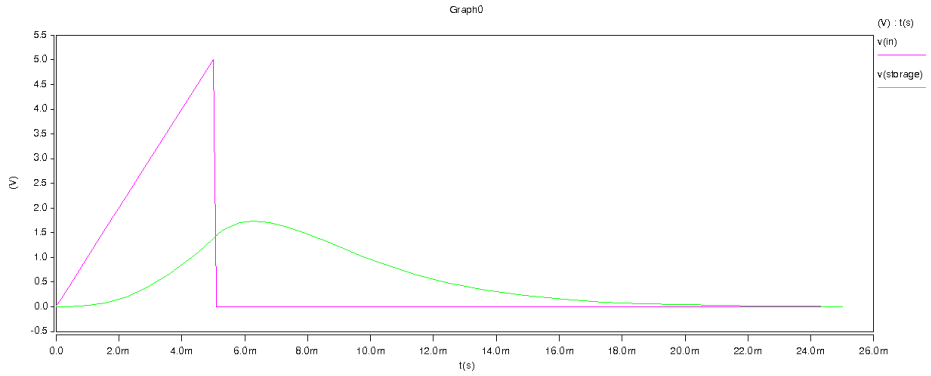

Figure 2.5. The critically damped response of the RLC circuit.

2.3.2. Under-damped Response

For the systems response to be under-damped the damping factor should be less than one. If the damping factor $\zeta = \frac{R}{2}\sqrt{\frac{C}{L}} < 1$, then the value of the capacitor $C < 2.716\,\mu$F. The attenuation coefficient $\alpha = 414$ for the given R and L values. Homogenous response of the system:

$$V_{\mathrm{CH}}(t) = Ate^{-\alpha t}\cos\omega_{\mathrm{d}}t + Be^{-\alpha t}\sin\omega_{\mathrm{d}}t \tag{2.25}$$

where $\omega_{\mathrm{d}} = \sqrt{\omega_0{}^2 - \alpha^2}$ is the damped natural frequency of the oscillation at which the system decays at. This is a parameter for only the under-damped case and the particular response of the system:

$$V_{\mathrm{CP}}(t) = r(t) + D \tag{2.26}$$

The value of D can be calculated if we substitute the particular response in Equation 2.25 $V_{\mathrm{CP}}(t)$ into equation 2.18, then $D = -1.8\,\mathrm{x}\,10^6 C$, here C is the value of the capacitor. By applying the initial conditions, the value of $A = 1.8\,\mathrm{x}\,10^6 C$ and $B = (745.2\,\mathrm{x}\,10^6 C - 1000)/\ \omega_{\mathrm{d}}$ here C indicates the value of the capacitor and ω_{d} indicates the damped natural frequency.

For $C = 2\ \mu$F, the response of the system is

$$V_{\mathrm{c}}(t) = 3.6te^{-414t}\cos\omega_{\mathrm{d}}t, + 2.02e^{-414t}\sin\omega_{\mathrm{d}}t + 1000t - 3.6 \tag{2.27}$$

For $C = 1\ \mu$F, the response of the system is

$$V_{\mathrm{c}}(t) = 1.8te^{-414t}\cos\omega_{\mathrm{d}}t, - 0.48e^{-414t}\sin\omega_{\mathrm{d}}t + 1000t - 1.8 \tag{2.28}$$

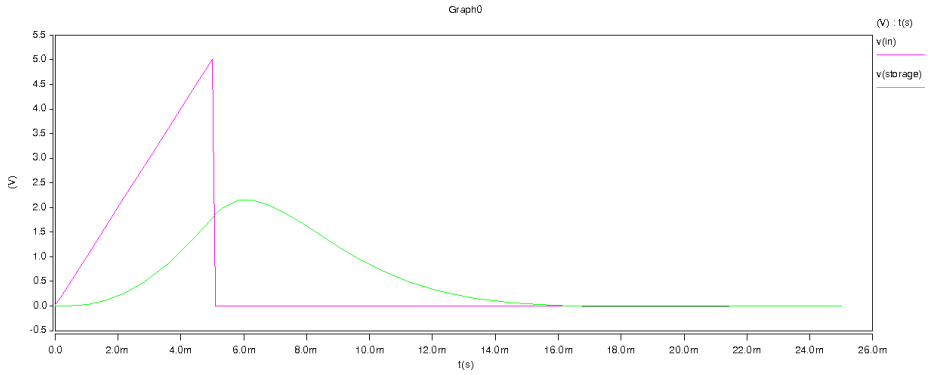

Figure 2.6. Under-damped response of the system when the value of the capacitor C = 2 μF.

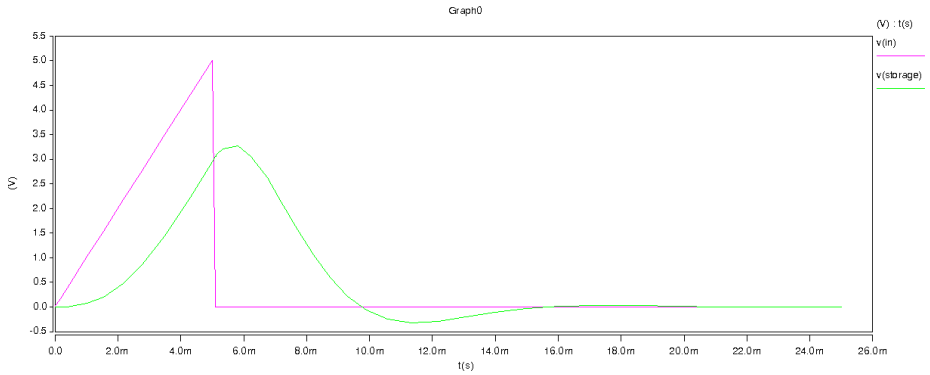

Figure 2.7. Under-damped response of the system when the value of the capacitor C = 1 μF.

2.3.3. Over-damped Response

For the systems response to be Over-damped the damping factor should be more than one. If the damping factor $\zeta = \frac{R}{2}\sqrt{\frac{C}{L}} > 1$, then the value of the capacitor $C > 2.716\,\mu$F. The attenuation coefficient $\alpha = 414$ for the given R and L values. Homogenous response of the system:

$$V_{\mathrm{CH}}(t) = Ae^{s_1 t} + Be^{s_2 t} \tag{2.29}$$

where $s_1 = -\alpha + \sqrt{\alpha^2 - {\omega_0}^2}$ and $s_2 = -\alpha - \sqrt{\alpha^2 - {\omega_0}^2}$ and the particular response of the system

$$V_{\mathrm{CP}}(t) = r(t) + D \tag{2.30}$$

Again the value of D can be calculated if we substitute the particular response in Equation 2.29 $V_{\mathrm{CP}}(t)$ into equation 2.18, then $D = -1.8 \times 10^6 C$, here C is the value of the capacitor.

For $C = 5\ \mu$F, the response of the system is

$$V_{\mathrm{c}}(t) = 9.304e^{-130.3t} - 0.304e^{-697.7t} + 1000t - 9 \tag{2.31}$$

For $C = 10\ \mu$F, the response of the system is

$$V_{\mathrm{c}}(t) = 18.0904e^{-59.12t} - 0.0904e^{-768.88t} + 1000t - 18 \tag{2.32}$$

In Figure 2.10 critically-damped, under-damped and over-damped responses are shown together. To get maximum peak voltage the under-damped case looks more suitable, however the value of the capacitor will be low and the value of that capacitor will not be sufficient to supply the STM 300 chip. More detailed analysis for the determination of the capacitor will be given in Section 3.3.

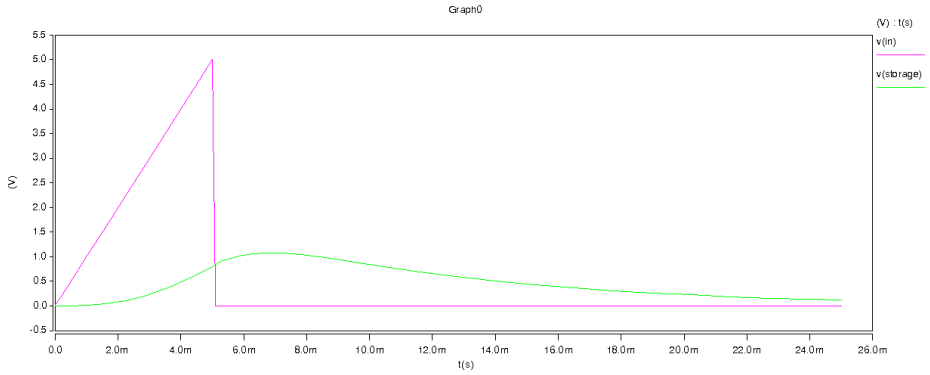

Figure 2.8. Over-damped response of the system when the value of the capacitor C = 5 μF.

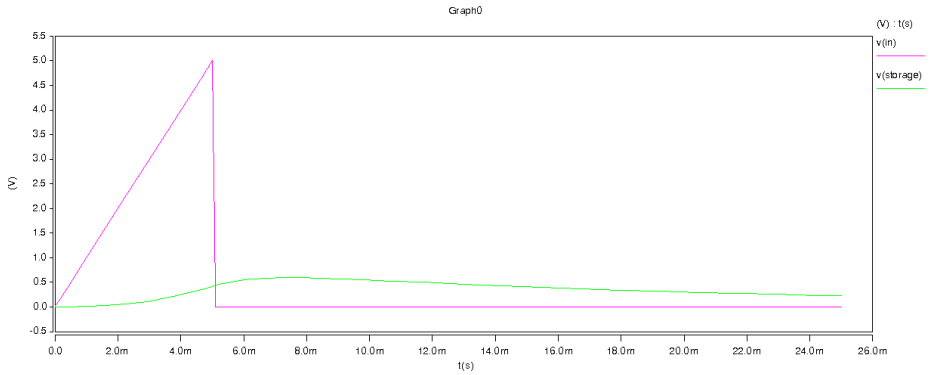

Figure 2.9. Over-damped response of the system when the value of the capacitor C = 10 μF.

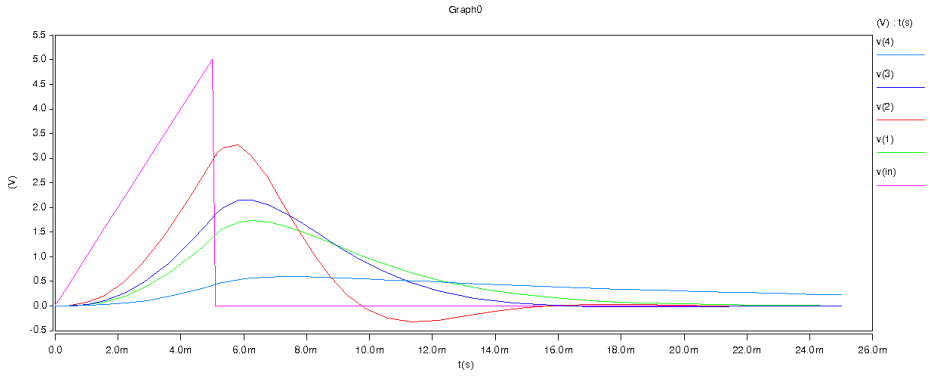

Figure 2.10. The comparison between critically-damped, under-damped and over-damped responses.

3. SIMULATION AND SYSTEM DESIGN

3.1. Simulation of Induced Voltage at the Coil by a Moving Magnet

The simulations of the moving magnet through the coil are made in the COMSOL Multiphysics environment. In the simulations the models that represent magnet and coil are in the 2D and axisymmetric, and modeling space is a rectangular region in the rz-plane bounded by the magnetic insulation boundary condition [18]. In the simulations different cases are examined e.g. by changing the dimensions of the magnet and the length or the radius of the coil. In the simulations, the dimensions of the magnets: radius and the height of the magnet five mm, the number of turn of the coil is 12000, the length of the coil is 2.5 cm, the width of the winding of the coil is 0.48 cm and the radius of the wire of the coil is 50 μm if the change of those parameters are not examined. In the first simulation, the effects of both the number of magnet and the velocity of the magnets on the peak voltage of the induced emf has been examined.

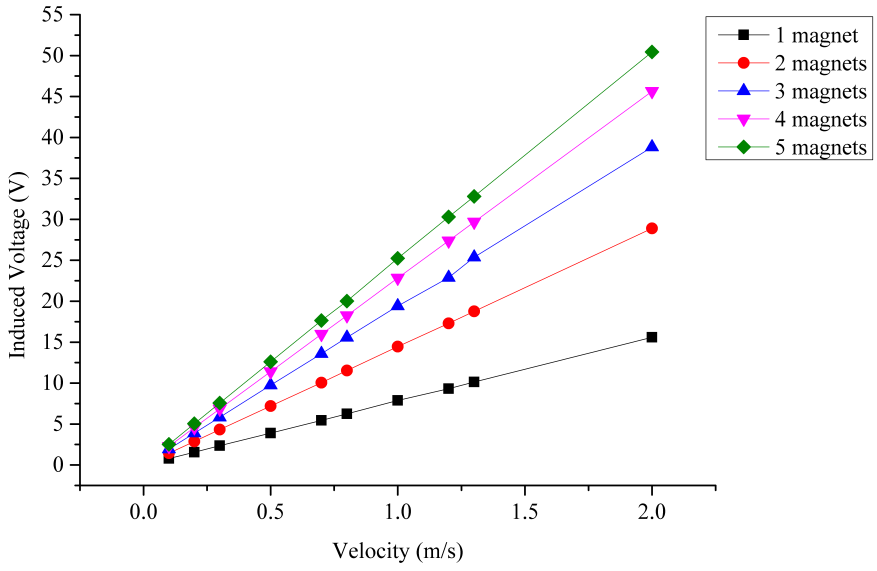

Figure 3.1. The graph of velocity of the magnet vs. the peak value of the induced voltage at the coil for different number of magnets.

As it can be seen from Figure 3.1 the peak value of the induced voltage is linear with the instant velocity of the magnet. However as the number of the magnet increases, the amount of increase in the induced emf decreases. The reason for this while adding a magnet increases the magnetic field but the added magnet will be farther away by one magnet's length for each time a new magnet is added, since the magnetic field of a bar magnet is inversely proportional to the cube of the distance from the magnet

$$B = \frac{2\mu_0 m}{z^3} \tag{3.1}$$

where z axis is align with the bar magnet. The decrease in the amount of increase in the induced voltage as we add more magnet can be seen in Figure 3.2. At some point adding more magnet will make no significant increase in the induced voltage.

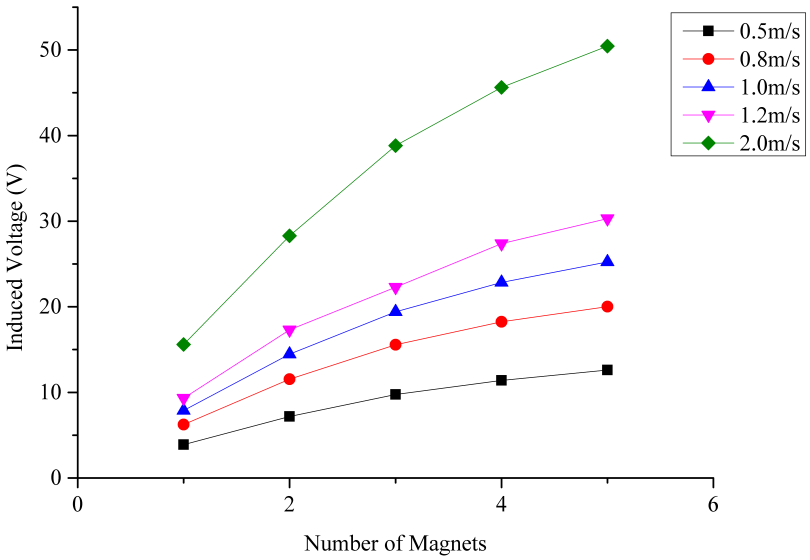

Figure 3.2. The graph of the number of magnets vs. induced voltage for different magnet velocity.

In the second and third simulation, how the peak voltage of the induced emf is changed with the number of turns of the coil has been examined. In the first case,

the number of turns of the coil is changed by changing only coil's length while the winding width of the coil is being kept constant. The simulation result for this case can be seen in Figure 3.3. As it can be seen in Figure 3.3 at some point the increase almost linear and after that point the induced voltage become almost constant. The reason for this, the magnetic field is inversely proportional to the cube of the distance from the center of the magnet. If the length of the coil is long enough such that when the magnet entering the coil, the closer part of the coil to the magnet experiences significant change of magnetic flux, while farther part experiences very low magnetic flux change, due to the very weak magnetic field strength at the farther part of the coil and while the magnet travels within the coil no emf will be induced at the coil. Thus, increasing the number of turns of the coil by only increasing the coil length, at some point, will not increase the peak value of the induced emf very much.

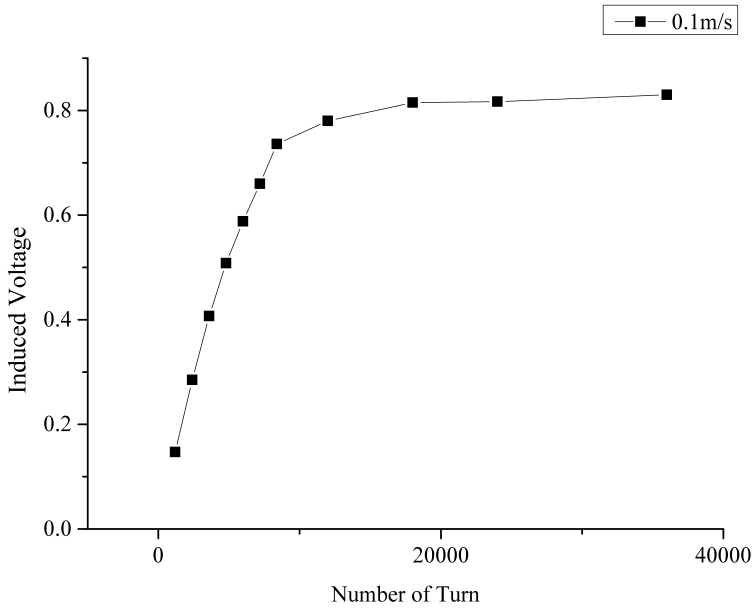

Figure 3.3. The graph of induced voltage vs. number of turns of the coil. In this case, the winding width of the coil is kept constant.

In the second case, the number of turns of the coil is changed by changing only the winding width of the coil while the length of the coil is being kept constant. The result for this case can be seen in Figure 3.4. In this case as the number of turns of the

coil increases, the peak value of the induced emf increases less than linearly. As the number of turns of the coil increases while the coil length is constant, the radius of the coil, r_{coil} increases. Since the resistance of the coil is the function of both the radius of the coil and the number of turns of the coil, the resistance of the coil increases more than linearly, thus the copper loss increases more than linearly.

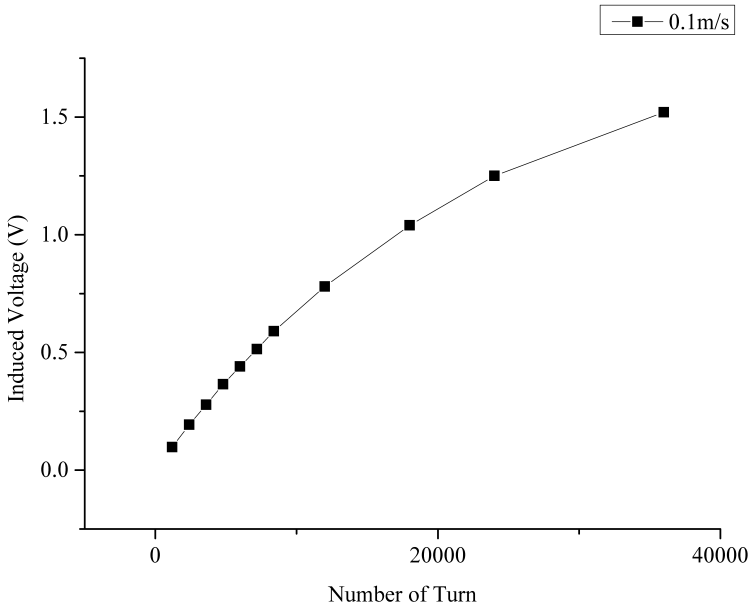

Figure 3.4. The graph of induced voltage vs. number of turns of the coil when the length of the coil is kept constant.

In the next simulation scenario, the effect of the change of inner radius of the coil is examined and the result is given in Figure 3.5. When the inner radius of the coil is slightly bigger than the radius of the bar magnet, almost all of the direction of the magnetic field lines, that are used for calculation of the flux, will be as same as direction of the moving magnet, assuming the north pole of the magnet closer to the coil . However, as the inner radius of the coil increases, the magnetic field lines, which are outside of the bar magnet, from the north pole to the south pole, which are in the opposite direction, cause to decrease in the magnetic flux despite of the increase in the area and these opposite-directioned magnetic field lines gets weaker as the distance increases from the magnet. Thus, the induced emf decreases less than linearly, as the

radius of the coil increases.

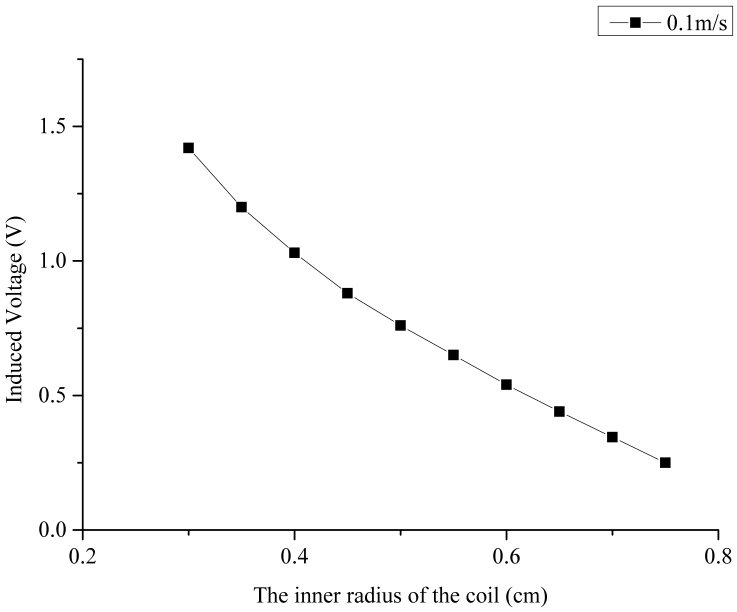

Figure 3.5. The graph of induced voltage versus the inner radius of the coil.

In the final simulation, only the radius of the magnet is changed while other parameters are kept being constant. As the radius of the magnet increases the number of the magnetic fields lines increases proportionally to the cross-sectional area of the bar magnet, which is squarely proportional to the radius of the magnet and as mentioned above as the radius of the magnet increases, the number of the opposite-directioned magnetic field lines, that passes through the cross-sectional area of the coil, decreases. Thus, the induced voltage at the coil increases more than it would increase squarely. The simulation result for this case is shown in Figure 3.6.

3.2. Determination of the Parameters of the Coil for the Motion Sensor

First some parameters of the coil are decided such that the dimensions of the coil will be as small as possible. The predicted parameters of the coil:

- the length of the coil, l_{coil} = 2-2.5 cm
- the outer diameter of the coil = 1 cm

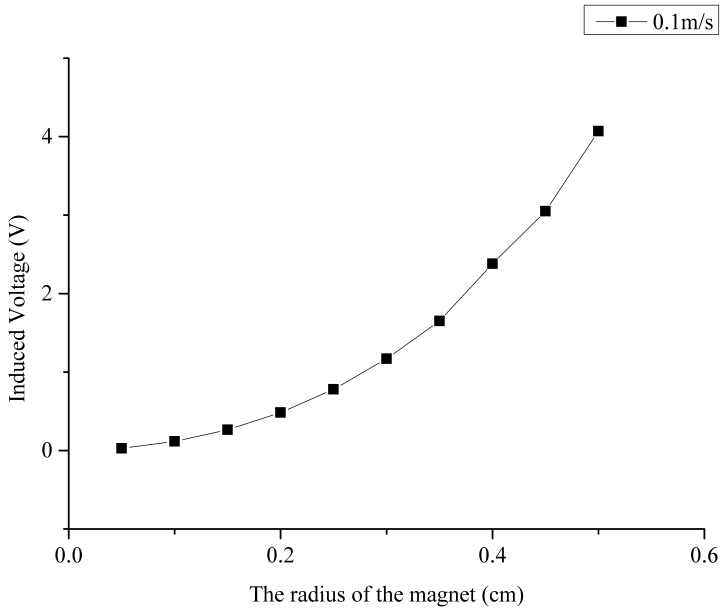

Figure 3.6. The graph of induced voltage versus the radius of the magnet.

- the inner diameter of the coil = 0.7 cm
- the diameter of the bar magnet = 0.5 cm
- the height of the bar magnet = 2 cm
- the diameter of the wire=0.0 6mm

The only parameter of the coil that left to be calculated is the number of turns of the coil, N. To calculate N, it needs to be decided that at what slowest velocity, the induced voltage will be sufficient to power up the STM 300 that is used in the motion sensor circuit. The slowest motion to be detected is the human walk. Since the sensor will be placed on the human wrist, it is needed to know what is the average speed of the human arm swing. The average speed of the human arm swing is around 0.3 cm/s [19], thus when the magnet's velocity around 0.3 cm/s the induced voltage should be around three volt to power up the STM 300 module, since the start up voltage of the module 2.6 V. According to the simulation the number of turns of the coil should be 12000 to meet the above requirement. The simulation result is shown in Figure 3.7.

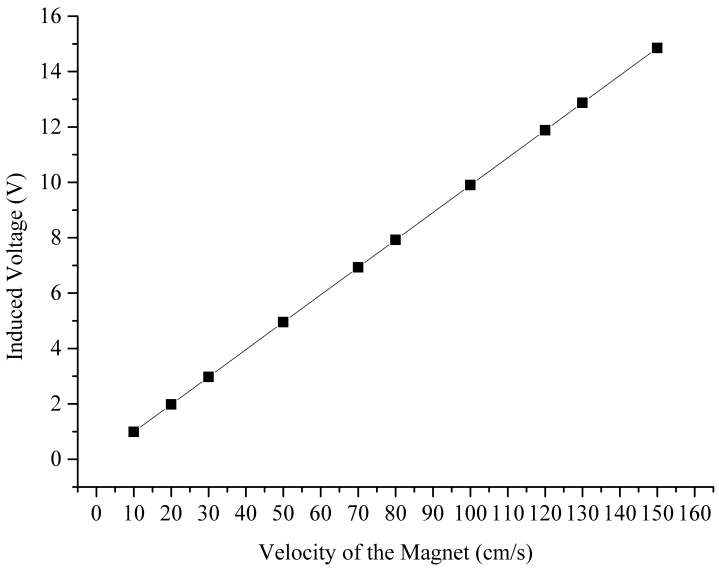

Figure 3.7. The simulation result for the first coil design.

But, we could not wind the coil that meets the specified requirements. The lowest possible inner diameter of the coil we could have is one centimeter and the thinnest wire we could have is 0.1 mm. The length of the coil and the number of turns of the of the coil are kept same as the previous case. Although, the there will be decrease in the induced voltage, since the inner diameter of the coil increases, this can be compensated by increasing the diameter of the magnet. In the final design of the coil, the coil parameters are:

- The number of turns of the coil, N = 12000
- the length of the coil, l_{coil} = 2.5 cm
- the outer diameter of the coil = 2 cm
- the inner diameter of the coil = 1 cm
- the diameter of the bar magnet = 0.635 cm
- the height of the bar magnet = 2.8575 cm
- the diameter of the wire = 0.1 mm

The simulation result of this coil is shown in Figure 3.8.

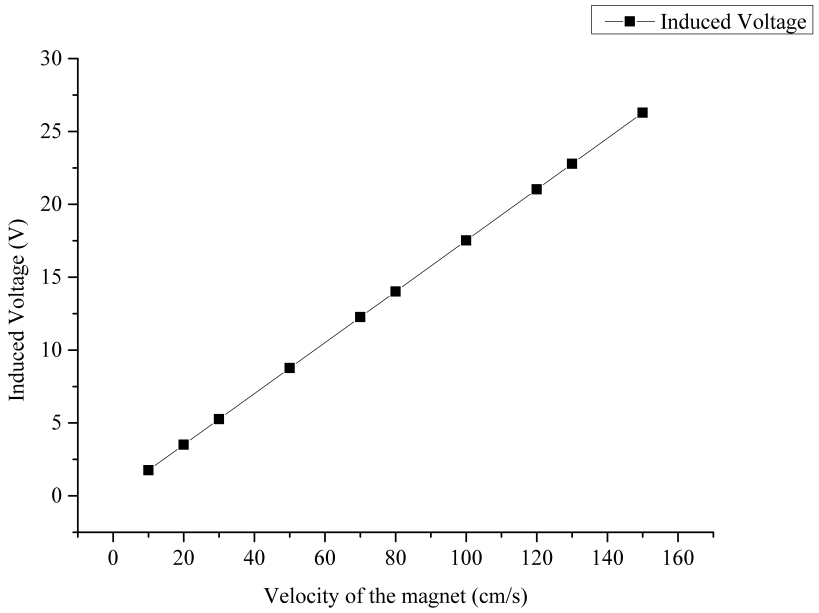

Figure 3.8. The simulation result for the final coil design.

3.3. Simulation and the Design of the Sensor Circuitry

The circuit that will power up the STM 300 module is a rectifier circuit and the analog input of the module is the output of the peak detectors. The utilize more harvested energy passive devices are used for both rectification and peak detection and the diodes are used in both circuits are the Schottky diode since it has a lower barrier voltage than that of p-n junction diode. The diodes that are used in the circuit are BAS40TW-7-F.

To simulate the circuit in Figure 2.4, the capacitor values for the storage and peak detector circuits are determined. As mentioned in Section 2.3, if the value of the capacitor is lower then, we can have more accurate value of the induced voltage peak. However, the lower values of the capacitor may not be sufficient for supplying the STM 300 module. The STM 300 module's start up voltage 2.6 V and the maximum supply voltage is 4.5 V. Charge needed for one measurement cycle without transmitting is 30 μC and the charge needed for the transmission is 100 μC. Thus, we need total approx-

imately 130 μC for the input reading and sending the transmission. The minimum capacitance we can have to function the module is about 28 μF if the supply is 4.5 V (130 μC/4.5 V = 28 μF) and we cannot sense the speeds that can produce voltage at the storage capacitor between 2.6 V and 4.5 V.

The smallest value of the capacitor that can power up the STM module, in the worst case that if the voltage at the storage capacitor is 2.6 V, is 50 μF (130 μC/2.6 V= 50 μF). We choose the closest standard value that is 47 μF.

We want to store most of the harvested energy in the storage capacitor, thus the capacitor value of the peak detectors are 1 μF. Almost 98 % of the harvested energy is stored at the storage capacitor and the two percent of the harvested energy is stored at the peak detector capacitors.

3.3.1. The Simulation of the Circuit

First the circuit in Figure 2.4 is simulated and the result is shown in Figure 3.9. Since the characteristic shape of the induced voltage looks like a single shot sinusoidal, the input signal in the simulation is a single shot sinus that have amplitude of 10 V and the signal width is 100 μsec.

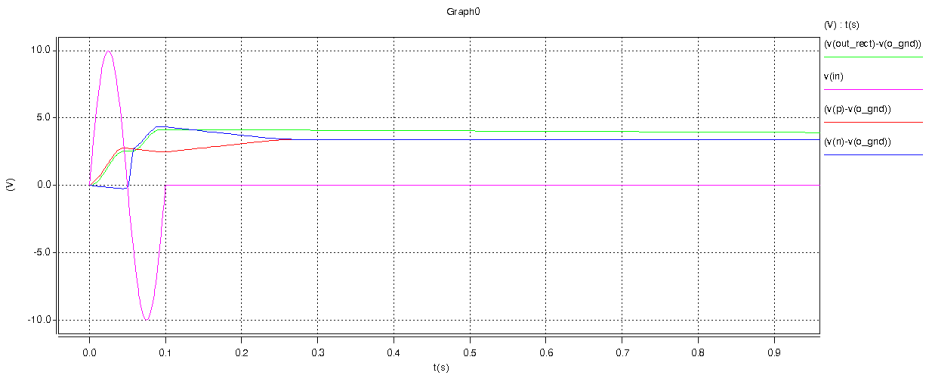

Figure 3.9. The simulation of the circuit in Figure 2.4.

In Figure 3.9 green line shows the voltage of the storage capacitor. Since the

storage capacitor is 47 μF, the system's response is over-damped and the settling time of the over-damped responses larger settling time than the that of others. Thus, the voltage of the storage capacitor rises during the negative cycle of the input. The red and the blue ones shows the voltage of the capacitor of the positive peak detector circuit and the capacitor of the negative peak detector circuit respectively. The rise in the positive peak detector's capacitor is caused by the references of the both positive and the negative peak detectors are the same. During the negative cycle the reference voltage become negative and when the negative peak detector's capacitor discharges, it will charge the positive peak detector's capacitor until the both capacitors have the same potential level. The decreases of the all capacitors is caused by the leakage of the capacitors. If the negative peak detector circuit is removed, the rise in the positive peak detector's capacitor will not be observed. This result is shown in Figure 3.10.

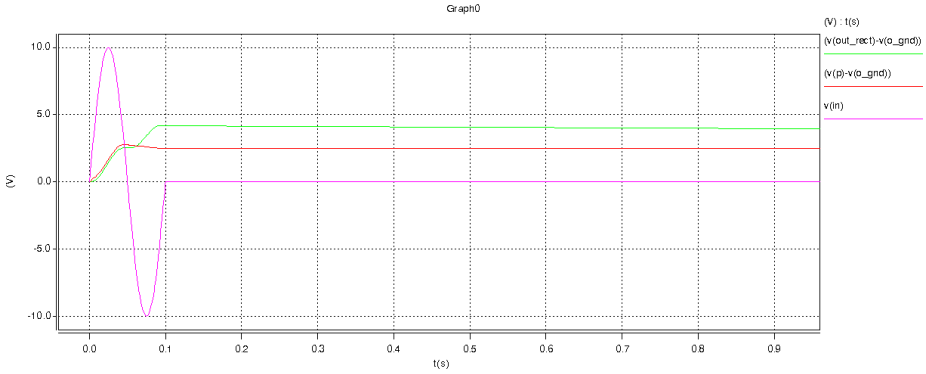

Figure 3.10. The simulation of the circuit in Figure 2.4 without the negative peak detector circuit.

The AC analysis of the circuit is shown in Figure 3.11. The natural frequency of the circuit is around 14 Hz but, the voltage does not reaches the maximum value at the resonant frequency. The reason for this the quality factor is very low which is less than one. The quality factor, Q, of an RLC circuit is:

$$Q = R\sqrt{\frac{C}{L}} = \frac{R}{\omega_0 L} \tag{3.2}$$

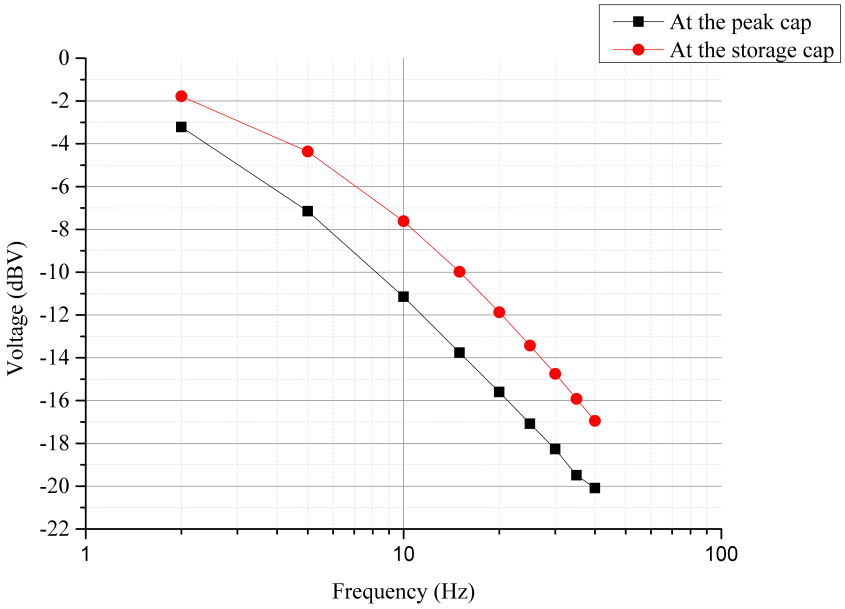

Figure 3.11. The AC analysis of the circuit in Figure 2.4.

In another simulation, how the voltages at the capacitors changes with the velocity of the magnet is examined. The simulation result is shown in Figure 3.12.

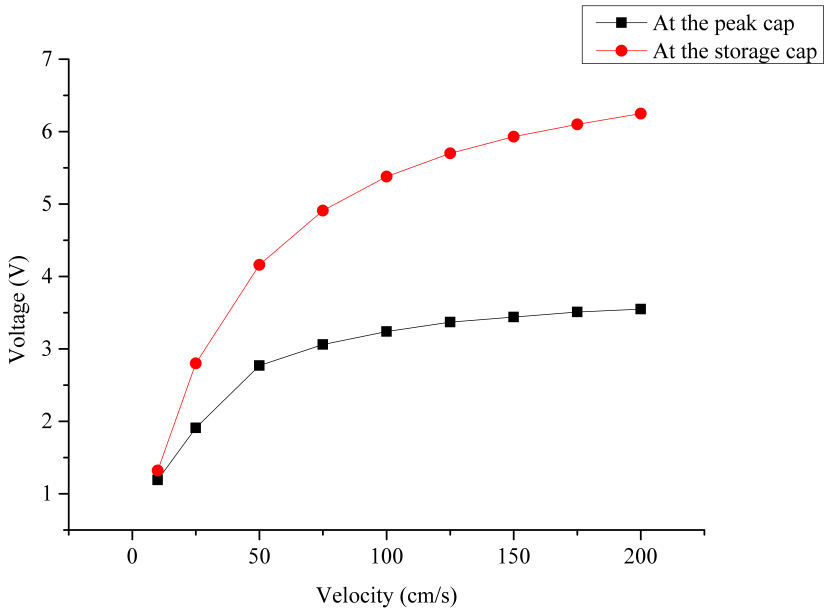

Figure 3.12. The simulation of the velocity of the magnet vs. the voltages at the capacitors.

Even though, the induced voltage at the coil increases linearly with the velocity of the magnet, but the voltages at the both the storage capacitor and the peak capacitor are not linear with the velocity of the magnet because of the very low quality factor.

3.3.2. The Design Process

For the system function well, we need the voltage at the peak capacitor to be linearly with the velocity of the magnet. The non-linearity in Figure 3.12 comes from very low quality factor of the circuit due to the high resistance of the coil. Since we cannot change the resistance of the coil without the changing the parameters of the coil we cannot improve the quality factor very much. However, we can improve the response of the peak capacitor by adding a series resistance between the positive output of the rectifier and the storage capacitor at the expense of the performance of the storage capacitor since adding a series resistor to the circuit worsen the quality factor.

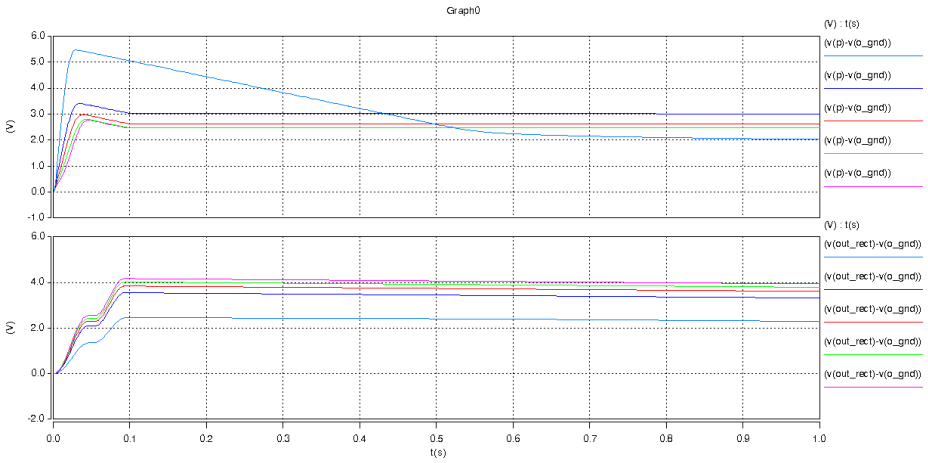

Figure 3.13. The simulation results for different value of the added series resistor.

In Figure 3.13, the light blue line for the series resistor is 2k ohms, the dark blue line for the series resistor is 1k ohms, the red one is for the 500 ohms, the green one is for the 100 ohms and the pink one is for there is no series resistor and the graph at bottom shows the voltages of the storage capacitors of the circuits and the other graph shows the voltages of the peak capacitors. As seen in Figure 3.13 as the value

of the series resistor increases the voltage at the peak capacitor increases while the voltage at the storage capacitor decreases.

We choose the value of the series resistor 500 ohms, to increase the performance of the peak detector at the expense of the almost 20 % voltage of the storage capacitor (0.5k/2.3k = 0.217).

Another problem we faced is if the input does not reach the peak value before the powering up the STM 300 module, most of the time the STM 300 module read the analog input wrong. To overcome this problem, a MOSFET switch is placed before the supply of the STM 300 module that switch will be open after a certain time. The delay is controlled by an RC circuit, The values of R1= 560k and C1 =1 μF. For the MOSFETs we choose ones with lower threshold value. The MOSFETs are 4562 which is N/P-channel pair with 0.6V threshold for the both pair.

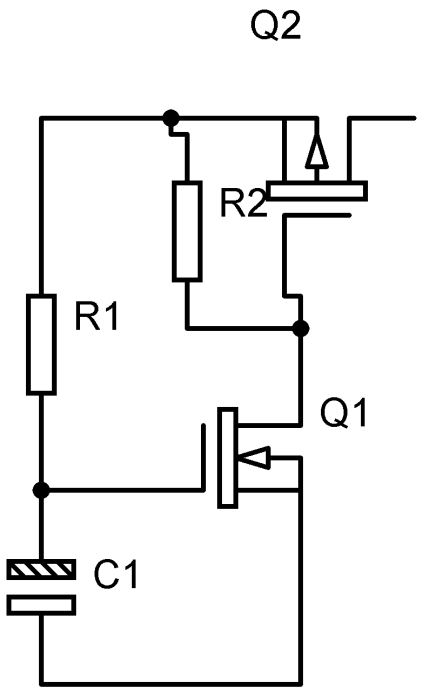

Figure 3.14. The MOSFET switch used for delay.

In Figure 3.15 the delayed output, the blue line, and the rectifier's output, the pink one, is shown. The delay is approximately 120ms.

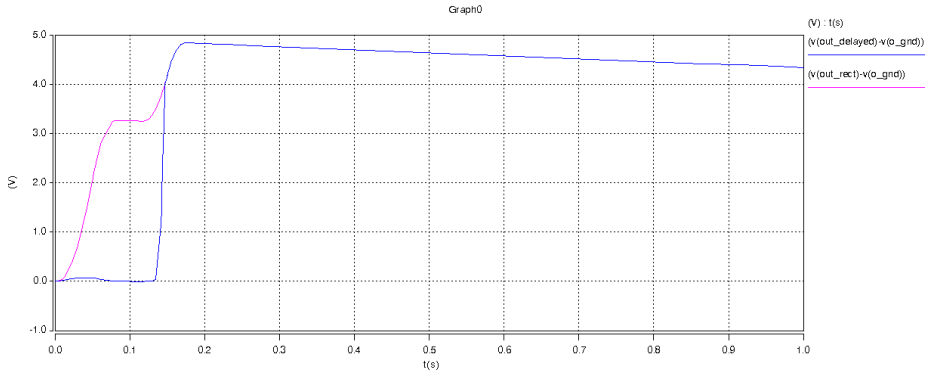

Figure 3.15. The output of the rectified signal and the delayed supply for the STM 300.

In the next step, since the maximum supply voltage of the STM 300 is 4.5 V, there is need for the over-voltage protection circuit for the STM 300, otherwise at the voltages above 4.5 V can burn the STM 300 module. The overvoltage protection part of the circuit consists of a resistance, a zener diode and an N channel MOSFET. The over-voltage protection circuit is shown in Figure 3.16.

The purpose of the resistor in the circuit is the limit the current of the zener diode. In the circuit, the value of the resistor is 100k ohms, and because of this high value the current that pass through the zener diode is very low and the zener diode operates below the knee voltage. The diode is 4.7 V zener diode and since the zener diode operates below the knee voltage, the maximum output of the circuit is around 4.5 V.

The final design step of the circuit is making sure that the output of the peak detector capacitor to fall in to the acceptable range that is the range of the analog measurement of the STM 300. STM 300 measure the analog input between 0.067V and 1.68V. At the slowest velocity that can power the STM 300 module, the value of the peak capacitor is 1.39V. We want this value closer to the minimum voltage

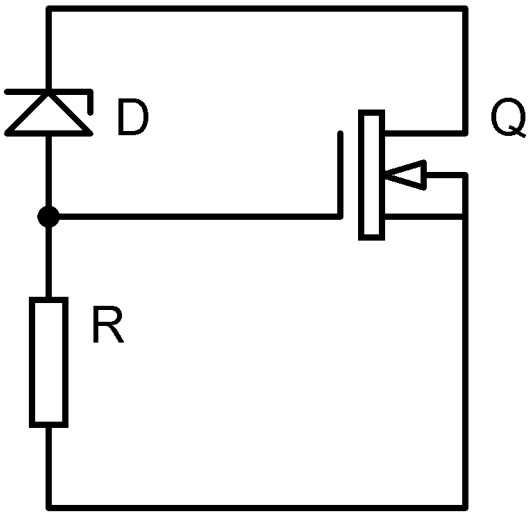

Figure 3.16. The over-voltage protection circuit.

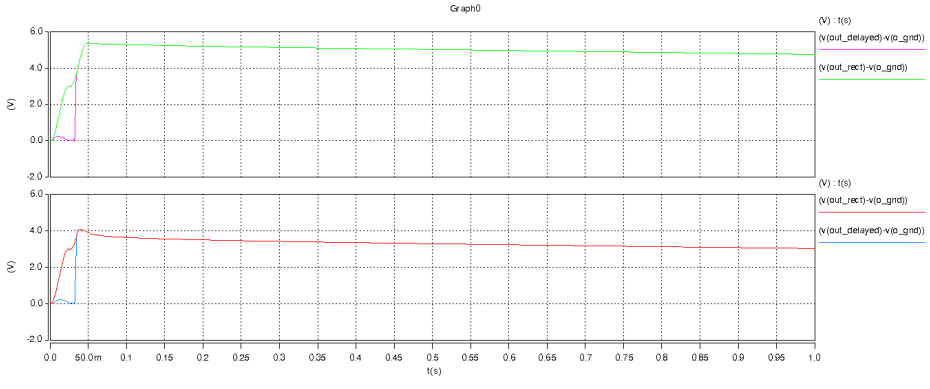

Figure 3.17. The comparison of the circuit without and with the overvoltage protection.

value of the STM 300's analog measurement range. This is accomplished by voltage division, by adding a series capacitor to the peak capacitor. The peak capacitor is 1 μF and the added capacitor is 10 μF, thus we divided the voltage of the peak by eleven. We need also resetting the peak value after each measurement. Resetting is done by a MOSFET switch, that will open after a certain time that is after the STM 300 measure the analog input, digitize it and transmit the data. There is also a series resistance of one megaohms between the peak detectors output and the input of the ADC of the STM 300, since the input impedance of the STM 300 is lower for the lower supply voltages.

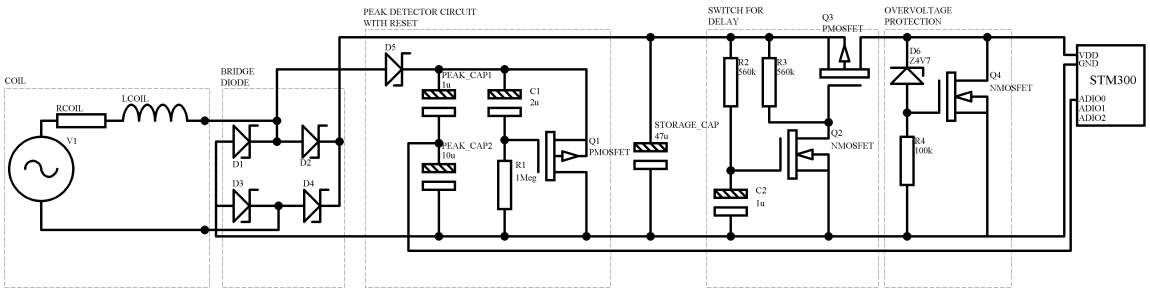

Figure 3.18. The complete schematic of the daily motion sensor harvesting circuit.

4. THE MEASUREMENTS AND DISCUSSION

In the previous two chapters, analysis and simulation were made to show the relationship between the velocity of the magnet and the peak value of the induced voltage for a magnet passes through coil system. The measurements can be split into two categories: The first is the measurements are done without the sensor circuit to verify the linear relation in the simulations and the second part of the measurements is the measurements done with the sensor circuit.

4.1. The Experiment Setup

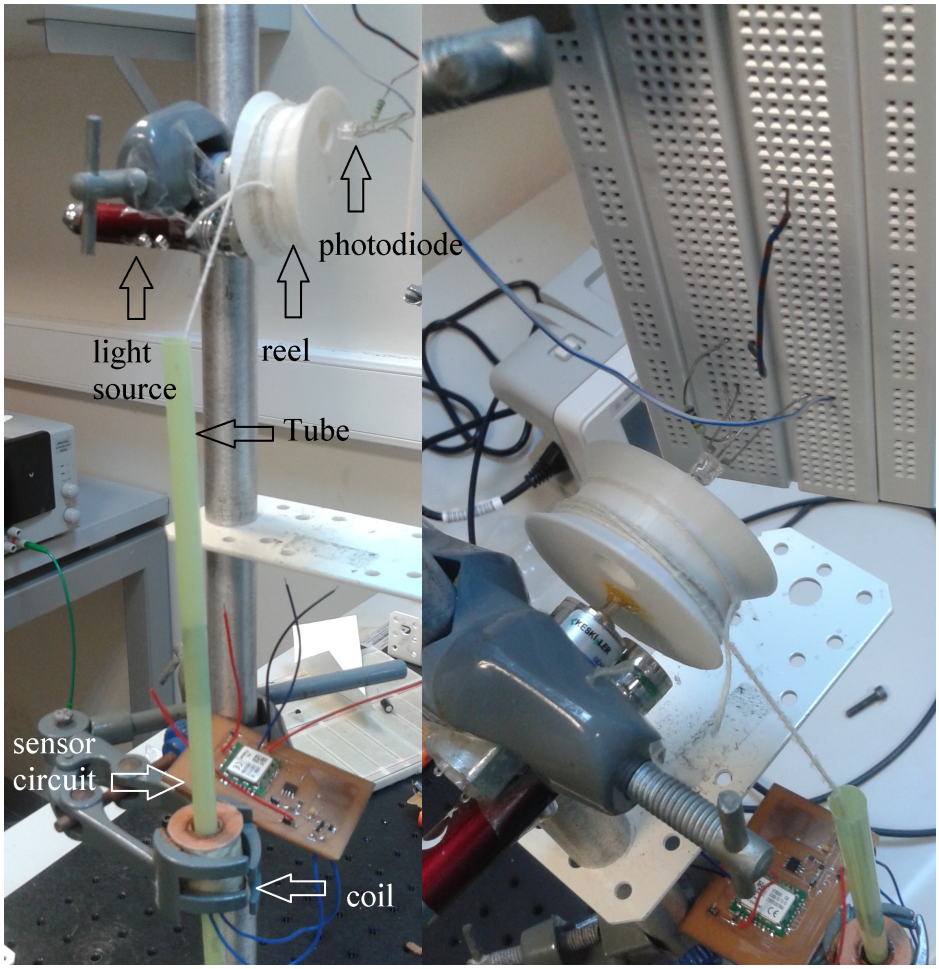

Figure 4.1. Experiment setup.

In the experiment setup, the reel is attached to a dc motor that pulls the magnet/ magnets at a constant velocity. The tube's axis is aligned with that of the coil to ensure that the magnet moves along the coil axis. The velocity of the magnet is measured opto-electronically. In the velocity measurement process, there is a hole at the reel that the light from the light source hits the photodiode once for the one period of the rotation of the reel. By examining the output of the photodiode, the period of the rotation can be measured that is the time between two peaks of the output of the photodiode.

4.2. Measurements Without the Sensor Circuit

In this section, the measurement results will be given for the peak of the induced voltage of the coil without the sensor circuit with respect to the velocity of the magnet. The induced voltage is monitored with an oscilloscope. Before mentioning the measurement results, the analysis of the accuracy of the measured induced voltage is made due to the loading effect. The impedance of the coil is a 1.8k ohms resistor is series with a 2.2 H inductor and the impedance of the probe is a one mega ohms resistor is parallel with a 10 pF capacitor.

$$V_{\text{measured}} = \frac{Z_{\text{probe}}}{Z_{\text{total}}} V_{\text{actual}} \tag{4.1}$$

where V_{measured} is the measured voltage, Z_{probe} is the impedance of the probe Z_{probe} is the total impedance of the probe and the coil and V_{actual} is the actual induced voltage.

$\frac{Z_{\text{probe}}}{Z_{\text{total}}} = 0.998$ for the frequencies lower than 1000 Hz and the phase shift is almost 3^0 for the specified range above. The measurement results are very close the actual values (The measurement error is less than 0.01%).

The given data is for the measurement results are for: the coil has 12000 turns and the both the diameter and the length of the magnet is five mm.

The amount of increase in the peak value decreases as the number of the magnets

Table 4.1. The measurement results for the coil with 12000 turns and the number of the magnet is one.

Velocity(cm/s)	Voltage(v)
43.1	1.40
46.3	1.48
53.2	1.72
56.8	1.84
62.5	1.96
72.5	2.28

Table 4.2. The measurement results for the coil with 12000 turns and the number of the magnet is two.

Velocity(cm/s)	Voltage(v)
44.0	2.65
49.1	2.96
59.1	3.68
61.1	3.76
65.0	4.00
74.2	4.40

Table 4.3. The measurement results for the coil with 12000 turns and the number of the magnet is three.

Velocity(cm/s)	Voltage(v)
42.5	3.36
48.5	3.85
56.1	4.56
60.0	4.74
67.5	5.36
75.0	5.92

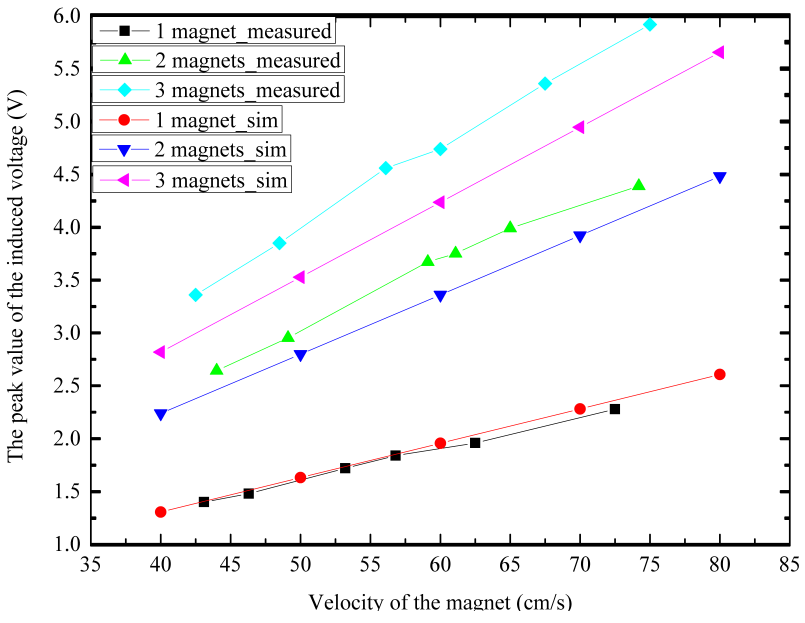

Figure 4.2. The simulation and the measurement results for the velocity of the magnet vs. the peak value of the induced voltage at the coil for different number of magnets.

increases as it is mentioned in Section 3.1. The next measurement results are for the magnets that are used in the sensor system. The data is recorded, again, without the sensor circuit. The coil that are used in the experiment has 12000 turns and the magnet has 0.635 cm diameter and the 0.9525 cm length.

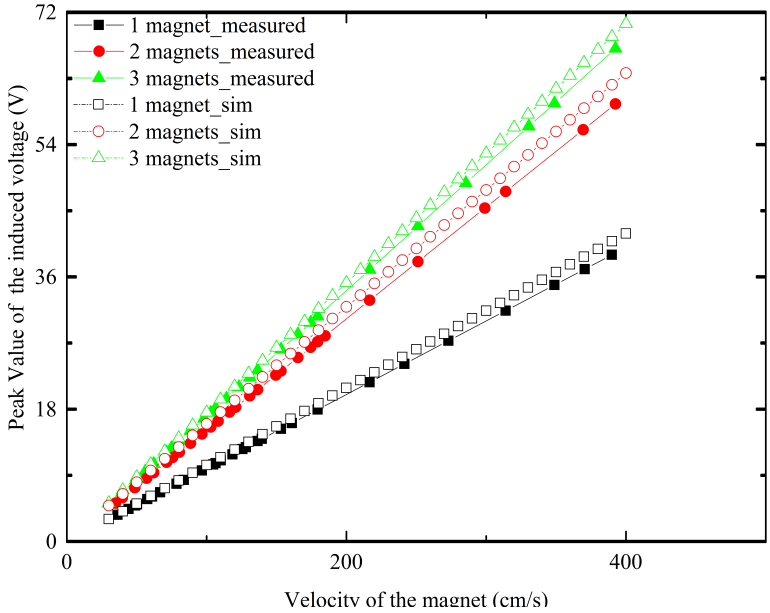

Figure 4.3. The simulation and the measurement result for the velocity of the magnet vs. the peak value of the induced voltage at the coil for different number of magnets.

In this experiment too, as the number of the magnet increases the increase in the peak value of the induced voltage decreases. As it can be seen in Figure 4.3 the simulation results are very close to the measurement results.

4.3. Measurements With the Sensor Circuit

The results for this experiment will be very different from the results in Section 4.2 since the most of the energy produced by the coil will be dissipated by the resistance of the coil, R_{coil}.

In the first experiment, the measurement results are for the circuit that is mentioned in Section 3.3.1. In this circuit, there is no series resistance added between the

Table 4.4. The measurement results of the data in Figure 4.3.

1 magnet		2 magnets		3 magnets	
Velocity (cm/s)	The peak voltage	Velocity (cm/s)	The peak voltage	Velocity (cm/s)	The peak voltage
36.29	3.63	34.89	5.30	39.50	6.75
44.22	4.42	39.75	6.04	49.45	8.46
48.93	4.89	48.68	7.40	56.07	9.59
50.32	5.03	57.09	8.68	62.18	10.63
57.61	5.76	62.18	9.45	71.36	12.20
60.97	6.10	71.36	10.85	74.76	12.78
66.81	6.68	75.66	11.50	80.51	13.77
78.50	7.85	80.51	12.24	88.45	15.12
83.73	8.37	88.45	13.44	98.13	16.78
96.62	9.66	96.62	14.69	102.95	17.60
104.67	10.47	102.95	15.65	106.44	18.20
106.44	10.64	108.28	16.46	114.18	19.52
110.18	11.02	116.30	17.68	123.14	21.06
118.49	11.85	120.77	18.36	130.83	22.37
125.60	12.56	130.83	19.89	136.52	23.34
128.16	12.82	136.52	20.75	139.62	23.90
136.52	13.65	149.52	22.73	153.17	26.19
139.56	13.96	153.17	23.28	158.85	27.13
153.17	15.32	165.26	25.12	165.26	28.26
161.03	16.10	174.44	26.51	170.42	29.12
179.43	17.94	179.43	27.27	174.44	29.83
216.55	21.66	184.71	28.08	179.43	30.68
241.54	24.15	216.55	32.92	216.55	37.03
273.04	27.30	251.20	38.18	251.20	42.96
314.00	31.40	299.05	45.46	285.45	48.81
348.89	34.89	314.00	47.73	330.53	56.52
370.52	37.05	369.41	56.15	348.89	59.66
389.95	39.00	392.50	59.66	392.50	67.12

output of the rectifier and the storage capacitor. The number of the magnet used in the experiment is three.

Table 4.5. The measurement result for the circuit in Section 3.3.1.

Velocity (cm/s)	The peak value of the induced voltage(V)
30.51	1.72
38.56	1.84
48.35	1.92
51.52	2.28
55.63	2.77
61.62	3.01
65.48	3.13
73.09	3.05
75.73	3.17
81.63	3.25
101.38	3.29
104.76	3.33

The characteristic of the peaks of the induced voltage in Figure 4.4 is piecewise linear for the velocity of the magnet between 30 cm/s and 70 cm/s, since the input impedance of the ADC is lower for the lower supply voltages. The peak value almost become constant when the velocity of the magnet exceeds 70 cm/s. In the second experiment, to reduce effect of the storage capacitor in the peak detector capacitor (in other words, to make the measured voltage and the velocity close to linear), the storage capacitor is placed after the switch for delay, not before it as in Figure 3.18 and the increase the reliability of the experiment, the experiment was repeated four times.

The linearity increases with respect to the previous experiment, but the lowest

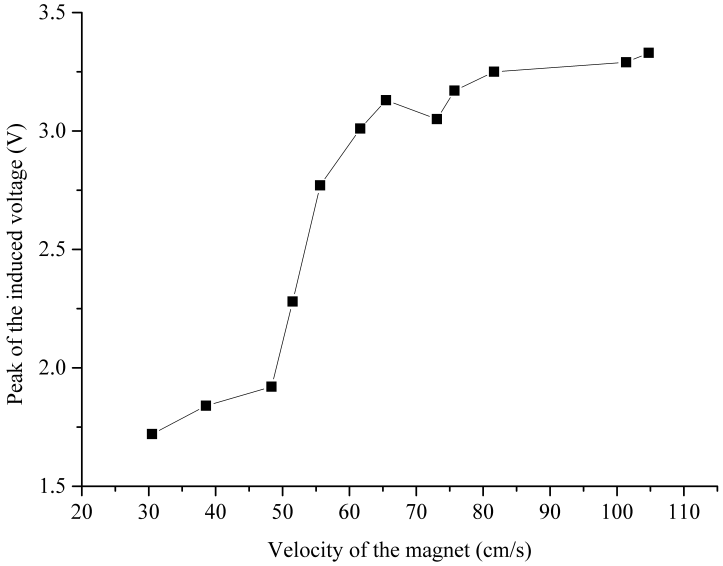

Figure 4.4. The graph of the measurement result for the circuit in Section 2.2.

Table 4.6. The measurement result for the circuit in Section 3.3.1.

I. Measurement		II. Measurement		III. Measurement		IV. Measurement		Average	
Peak	Velocity	Peak	Velocity	Peak	Velocity	Peak	Velocity	Peak	Velocity
3.88	57.61	4.20	56.58	4.37	57.61	4.20	58.69	4.16	57.62
4.85	60.97	4.85	63.43	4.85	63.43	4.85	62.18	4.85	62.50
5.18	66.81	5.34	69.01	4.85	66.81	5.01	69.78	5.09	68.10
6.31	78.50	6.63	79.49	5.98	76.59	6.31	78.50	6.31	78.27
8.25	83.73	8.25	89.71	8.25	89.71	8.09	86.03	8.21	87.30
10.35	96.62	10.03	93.73	9.86	93.73	10.35	93.73	10.15	94.45
11.00	104.67	11.00	104.67	10.51	104.67	10.67	106.44	10.79	105.11
11.32	106.44	11.00	104.67	11.48	106.44	11.00	104.67	11.20	105.55
11.64	110.18	11.48	114.18	11.16	110.18	11.48	110.18	11.44	111.18
11.97	118.49	12.13	118.49	12.13	123.14	11.97	114.18	12.05	118.58
12.78	125.60	12.61	125.60	12.29	123.14	12.45	120.77	12.53	123.78
13.10	128.16	12.94	130.83	13.10	128.16	13.26	133.62	13.10	130.19
13.75	136.52	13.91	139.56	13.91	136.52	13.42	133.62	13.75	136.55
14.07	139.56	13.91	139.56	14.07	142.73	14.07	142.73	14.03	141.14
14.72	153.17	14.88	157.00	14.55	153.17	14.72	153.17	14.72	154.13
15.20	161.03	15.20	157.00	15.85	161.03	15.69	157.00	15.48	159.01
17.63	179.43	17.63	179.43	17.63	179.43	17.63	179.43	17.63	179.43
19.08	216.55	19.08	216.55	19.08	216.55	19.08	216.55	19.08	216.55
21.19	241.54	21.19	241.54	21.19	241.54	21.19	241.54	21.19	241.54
22.16	273.04	22.16	273.04	22.16	273.04	22.16	273.04	22.16	273.04
24.90	314.00	24.90	314.00	24.90	314.00	24.90	314.00	24.90	314.00
25.71	348.89	25.71	348.89	25.71	348.89	25.71	348.89	25.71	348.89

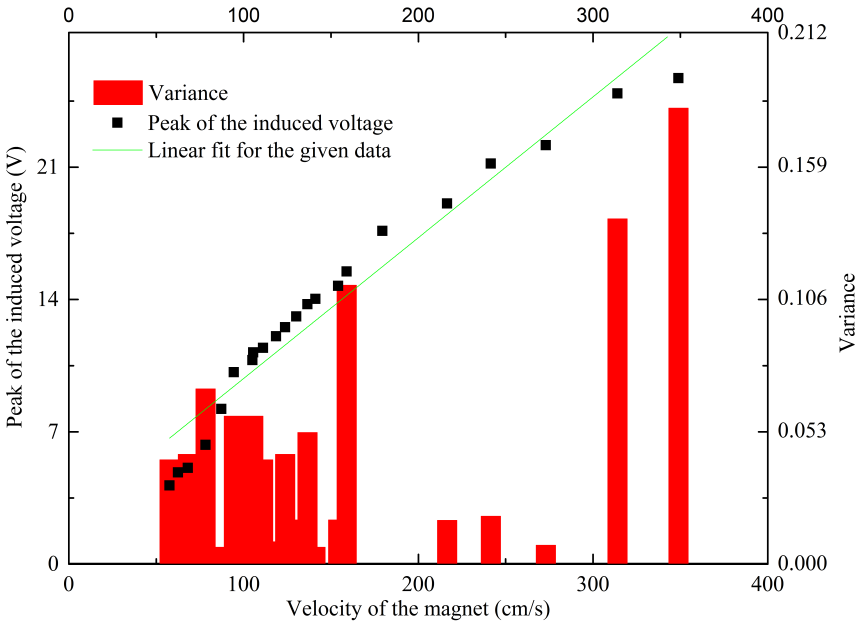

Figure 4.5. The graph of average data in Table 4.6.

detectable velocity of the magnet is near 50 cm/s, while the lowest detectable velocity of the magnet is around 30 cm/s in the previous experiment.

In third, the final, experiment, a different approach is used to make the relationship between the velocity and the induced voltage. A series resistance is added between the output of the rectifier and the storage capacitor as it is discussed in section 3.3.2.

The linearity increases with respect to the first experiment and the minimum detectable velocity of the magnet is around 35 cm/s, while the minimum detectable velocity of the magnet is around 30 cm/s in the first experiment.

The slope of the linear line is 0.04 V.s/cm. The data in Figure can be considered as piecewise linear. For the velocity range between 35 cm/s and 100 cm/s the slope is 0.087 V.s/cm and the slope for the velocity bigger than 100 cm/s is 0.034 V.s/cm.

The velocity of the magnet can be calculated using the graph in Figure 4.8. The graph in Figure 4.8 is piecewise linear whose slope is 130 cm/s.V for the ADC input

Table 4.7. The measurement result for the last experiment.

I. Measurement		II. Measurement		III. Measurement		IV. Measurement		Average	
Peak	Velocity	Peak	Velocity	Peak	Velocity	Peak	Velocity	Peak	Velocity
1.39	34.89	1.39	35.08	1.39	35.08	1.24	35.08	1.35	35.04
2.17	39.50	2.01	39.75	2.17	40.00	2.09	40.26	2.11	39.88
2.94	49.45	2.86	48.68	2.63	48.31	2.55	48.31	2.75	48.69
3.09	56.07	3.56	57.09	3.48	56.07	3.02	55.09	3.29	56.08
3.64	62.18	4.25	62.18	3.71	61.57	3.71	59.81	3.83	61.43
5.03	71.36	4.80	71.36	4.95	70.56	4.64	70.56	4.85	70.96
5.03	74.76	5.03	75.66	5.18	73.88	5.26	73.88	5.12	74.55
5.34	80.51	5.34	80.51	5.65	81.56	5.34	81.56	5.41	81.04
6.11	88.45	6.03	88.45	5.96	87.22	5.72	86.03	5.96	87.54
6.26	98.13	6.34	96.62	6.11	96.62	6.42	99.68	6.28	97.76
6.50	102.95	7.04	102.95	6.50	102.95	6.65	102.95	6.67	102.95
7.04	106.44	6.81	108.28	7.12	110.18	7.12	110.18	7.02	108.77
7.35	114.18	7.19	116.30	7.50	116.30	7.04	110.18	7.27	114.24
7.43	123.14	7.58	120.77	7.73	123.14	7.58	123.14	7.58	122.55
7.73	130.83	7.73	130.83	7.35	125.60	7.27	123.14	7.52	127.60
7.81	136.52	7.89	136.52	8.28	139.56	8.28	136.52	8.06	137.28
7.89	136.52	8.43	139.56	8.35	139.56	8.43	142.73	8.28	139.59
9.05	153.17	8.82	149.52	8.74	153.17	9.13	153.17	8.93	152.26
8.51	153.17	8.82	153.17	8.97	157.00	8.51	153.17	8.70	154.13
9.51	165.26	9.51	165.26	9.20	165.26	9.28	165.26	9.38	165.26
9.51	165.26	9.28	174.44	9.36	165.26	9.28	165.26	9.36	167.56
9.67	174.44	9.67	179.43	9.51	174.44	9.51	174.44	9.59	175.69
9.75	179.43	9.98	184.71	9.98	184.71	9.82	184.71	9.88	183.39
10.36	216.55	10.98	216.55	10.98	216.55	11.06	216.55	10.85	216.55
11.99	251.20	11.52	251.20	11.52	251.20	12.45	251.20	11.87	251.20
13.92	285.45	13.61	299.05	12.76	299.05	13.84	285.45	13.54	292.25
14.93	330.53	14.08	314.00	14.54	330.53	14.54	330.53	14.52	326.39
14.77	348.89	15.55	369.41	16.01	369.41	15.93	369.41	15.57	364.28
18.18	392.50	17.87	392.50	18.18	392.50	17.79	392.50	18.00	392.50

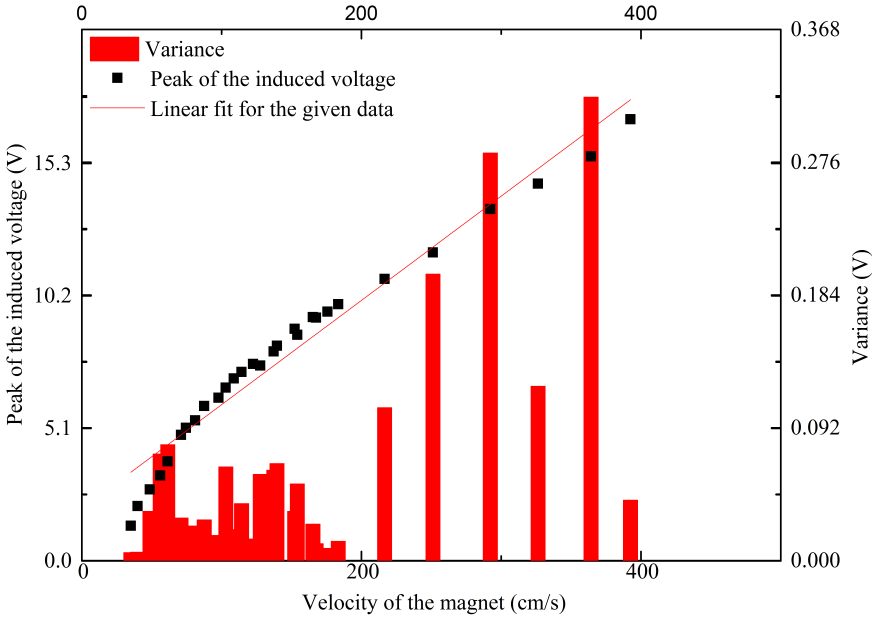

Figure 4.6. The graph of average data in Table 4.7.

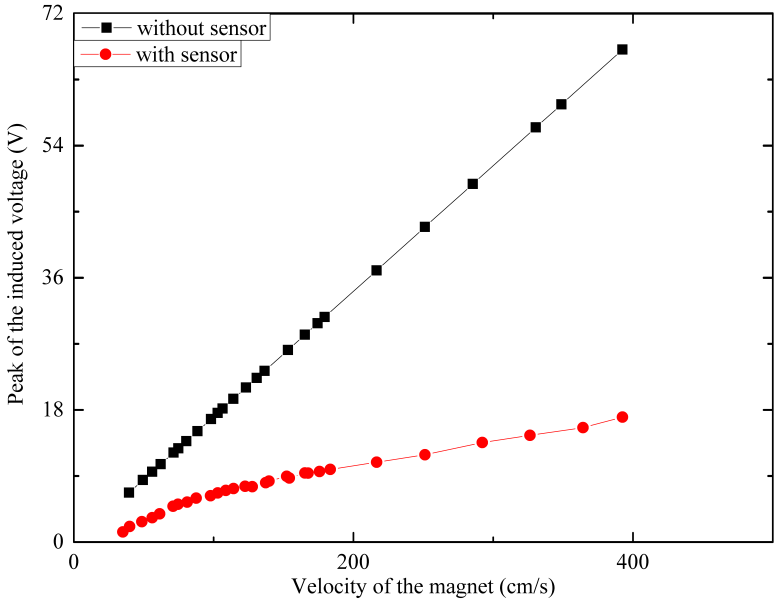

Figure 4.7. The peak of the induced voltage at the coil with and without the sensor circuit.

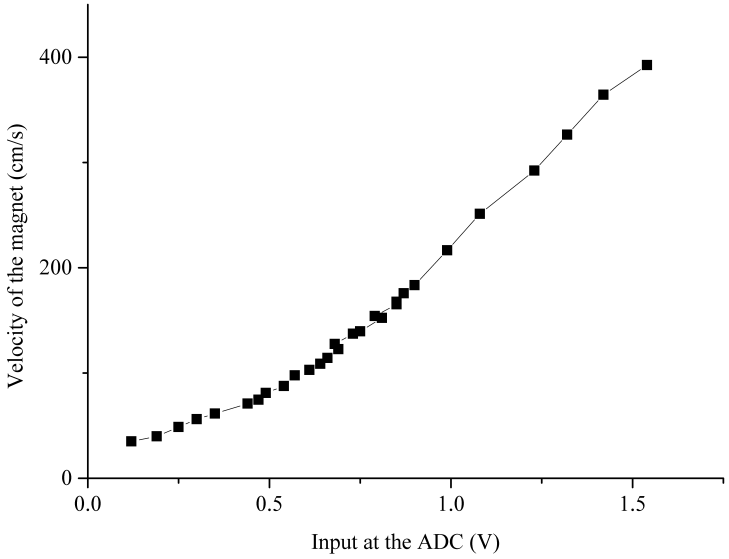

Figure 4.8. The graph of input at the ADC vs. the velocity of the magnet.

values between 0.12 V and 0.55 V, and for the ADC values higher than 0.55 V the slope of the graph is around 318 cm/s V. The slopes are found using linear fit using the OriginLab program [20]. Equation for the first line is

$$y = 130x + 19 \tag{4.2}$$

and the other linear line is

$$y = 318x - 97 \tag{4.3}$$

the velocity of the magnet can be calculated by these equations.

4.4. The Application of the Sensor

The system utilizes human motion to harvest energy. The sensor can be placed to human wrist like in Figure 4.8 that energy can be harvested by swinging the arm

during the walk or run and these motions can be sensed. The experiments were done for the different speed of human walking and running. All the given data for the incoming telegrams is in hexadecimal.

Table 4.8. The incoming telegrams for the walking speed of 60cm/s.

	Incoming Telegram				Calculated Velocity(cm/s)			
I. Experiment	21	22	1D	1D	49.60	50.52	46.86	46.86
II.Experiment	20	1E	23	21	48.69	47.78	51.43	49.60
III.Experiment	22	1B	24	22	50.52	44.12	52.35	50.52
IV.Experiment	23	21	1C	22	51.43	49.60	45.03	50.52

The average calculated speed of the data in Table 4.8 is 49.09 cm/s.

Table 4.9. The incoming telegrams for the walking speed of 80cm/s.

	Incoming Telegram				Calculated Velocity(cm/s)			
I. Experiment	27	1B	29	22	55.09	44.12	56.92	50.52
II.Experiment	26	34	24	29	54.17	66.97	52.35	56.92
III.Experiment	30	22	2C	26	63.32	50.52	59.66	54.17
IV.Experiment	28	21	29	36	56.00	49.60	56.92	68.80

The average calculated speed of the data in Table 4.9 is 56.00 cm/s.

The average calculated speed of the data in Table 4.10 is 76.74 cm/s.

The average calculated speed of the data in Table 4.11 is 94.31 cm/s.

The calculated speeds and the speeds of the walking or running are different from each other, since the calculated speeds are not the speed of walking or running, they are, in fact, the speed of the arm swing. For both walking and running, the speed of

Table 4.10. The incoming telegrams for the running speed of 100cm/s.

	Incoming Telegram				Calculated Velocity(cm/s)			
I. Experiment	44	3D	42	3A	81.60	75.20	79.77	72.46
II.Experiment	40	3D	46	38	77.94	75.20	83.42	70.63
III.Experiment	42	3A	40	39	79.77	72.46	77.94	71.54
IV.Experiment	44	38	46	3C	81.60	70.63	83.42	74.28

Table 4.11. The incoming telegrams for the running speed of 130cm/s.

	Incoming Telegram				Calculated Velocity(cm/s)			
I. Experiment	5C	4A	59	48	108.49	87.08	101.78	85.25
II.Experiment	52	46	5A	46	94.39	83.42	92.57	83.42
III.Experiment	5D	48	5C	50	110.72	85.25	108.49	92.57
IV.Experiment	56	4B	5B	49	95.07	87.99	106.25	86.17

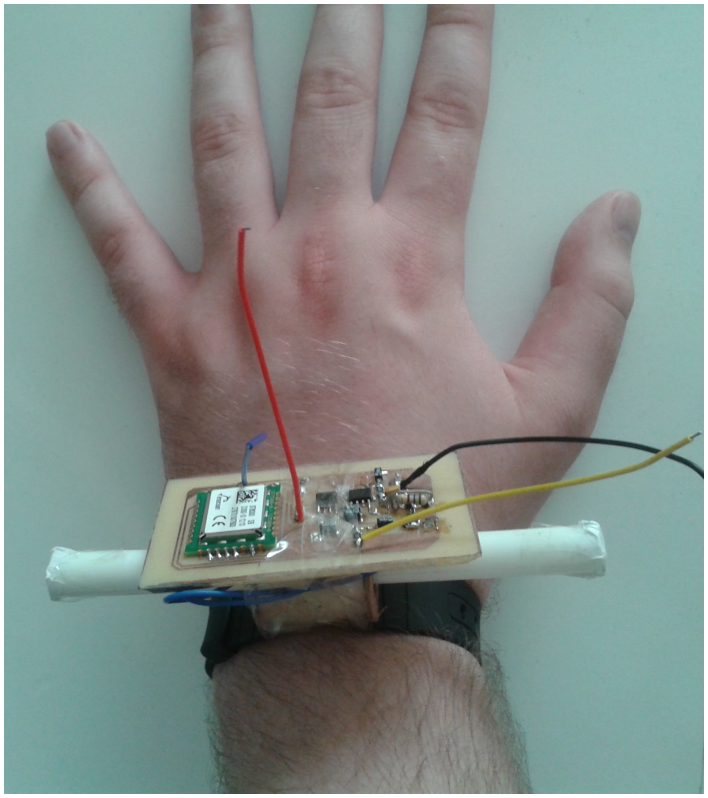

Figure 4.9. The designed motion sensor, placed on the wrist.

the arm swing is more close to motion speed for the lower speed of the motion, since for the lower motion speed the frequency of the arm swing is higher [19].

In another experiment the sensor is attached to the top of the rigid rod that has length of 80 cm, for modeling human fall. The rigid moves like in Figure 4.9. In the experiment, sensor only send one telegram during the fall.

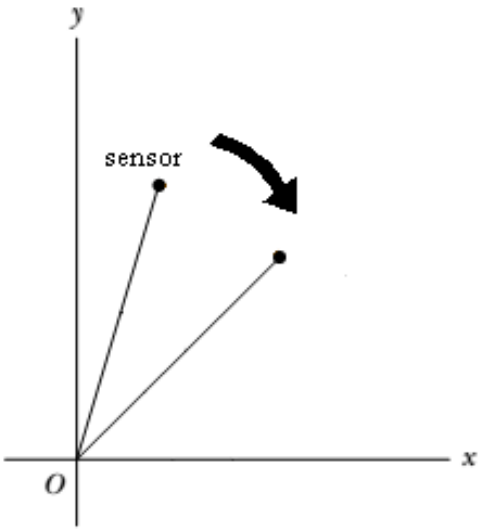

Figure 4.10. The fall detection experiment.

Table 4.12. The incoming telegram for the fall experiment.

	Incoming Telelgram	Calculated Velocity(cm/s)
I. Experiment	38	70.63
II.Experiment	36	68.80
III.Experiment	26	54.17
IV.Experiment	33	66.06

During the fall only one telegram is send while, for walking and running the number of incoming telegrams depends on the duration of the motion.

5. CONCLUSIONS

In this study, the linear relationship between the velocity of the magnet and the peak of induced voltage at the coil is shown through calculations, simulations and experiments. A system is designed that harvest energy from moving magnet through the coil and sense the instant velocity of the magnet by using the harvested energy at the same time. A motion sensor, that utilizes human motion for the energy harvesting, is realized to sense certain daily motions and the sensor is tested whether it can function well or not in the tests. It is seen that, in the experiments, different speeds of arm swing can be distinguishable from each other.

5.1. Future Works

The current motion sensor can sense speed as low as 35 cm/s and for some cases this speed is not low enough. One of the future research will be lowering the minimum sensible velocity magnet such as 10 cm/s. In the mathematical analysis, the effect of some parameters are not included: such as the length of the coil, the length of the magnet and the thickness of the coil wire. Developing more sophisticated mathematical model for the induced voltage at the coil will be another step for the future work. One of the drawback of this design is the velocity can be measured in only one direction. To detect the multi-directioned motion a new mechanical model will be designed. Another future work will be determination of different possible application area of the motion sensor. For example, the possible use of the motion sensor as a wireless and batteryless gamepad.

REFERENCES

1. Sari, I., T. Balkan and H. Kulah, "Optoelectronic CMOS Power Supply Unit for Electrically Isolated Microscale Applications", *Sensors and Actuators A*, Vol. 145, pp. 405–413, 2008.

2. Jones, P. G., M. J. Tudor, S. P. Beeby and N. M. White, "An electrormagnetic, vibration-powered generator for intelligent sensor systems", *Sensors and Actuators A*, Vol. 110, pp. 344–349, 2004.

3. James, E. P., M. J. Tudor, S. P. Beeby, N. R. Harris, P. G. Jones, J. N. Ross and N. M. White, "An investigation of self-powered systems for condition monitoring applications", *Sensors and Actuators A*, Vol. 110, pp. 171–174, 2004.

4. Gherca, R. and R. Olaru, "Harvesting Vibration Energy by Electromagnetic Induction", *Annals of the University of Craiova, Electrical Engineering series*, Vol. 35, pp. 7–12, 2011.

5. Zhu, D., S. Roberts, M. J. Tudor and S. P. Beeby, "Design and experimental characterization of a tunable vibration-based electromagnetic microgenerator", *Sensors and Actuators A*, Vol. 158, pp. 284–293, 2010.

6. Ching, N., H. Wong, W. Li, P. Leong and Z. Wen, "A laser-micromachined multimodal resonating power transducer for wireless sensing systems", *Sensors and Actuators A*, Vol. 97, pp. 685–690, 2002.

7. Kulah, H. and K. Najafi, "An electromagnetic micro power generator for low-frequency environmental vibrations", *Micro Electro Mechanical Systems, 17th IEEE International Conference on. (MEMS)*, pp. 237 – 240, 2004.

8. Williams, C., C. Sherwood, M. A. Harradine, P. H. M. T. S. Birch and R. B. Yates, "Development of an electromagnetic micro-generator", *IEE Proceedings, Circuits,*

Devices and Systems, Vol. 148, No. 6, pp. 337 – 342, 2001.

9. Spreemann, D., Y. Manoli, B. Folkmer and D. Mintenbeck, "Non-resonant vibration conversion", *Journal of Micromechanics and Microengineering*, Vol. 16, No. 9, p. S169, 2006, http://stacks.iop.org/0960-1317/16/i=9/a=S01.

10. Mann, B. P. and N. D. Sims, "Energy harvesting from the nonlinear oscillations of magnetic levitation", *Journal of Sound and Vibration*, Vol. 319, pp. 515–530, 2009.

11. Jonnalagadda, A. S., *Magnetic Induction Systems to Harvest Energy from Mechanical Vibrations*, Master's Thesis, MIT, 2007.

12. Mitcheson, P., E. Yeatman, G. Rao, A. Holmes and T. Green, "Energy Harvesting From Human and Machine Motion for Wireless Electronic Devices", *Proceedings of the IEEE*, Vol. 96, No. 9, pp. 1457–1486, Sept, 2008.

13. Alternative Energy, *Harvesting Ambient Energy from Nature*, 2009, http://www.alternative-energy-news.info/harvesting-ambient-energy-nature/, accessed on September 2013.

14. Enocean, *User Manual V1.35*, July 2013, http://www.enocean.com/fr/enocean_modules/stm-300-user-manual-pdf/, accessed on November 2013.

15. Pollack, G. L. and D. R. Stump, *Electromagnetism*, Addison Wesley, San Francisco, USA, 2002.

16. G. L. Pollack and D. R. Stump, *Magnetic Field of a Bar Magnet*, 2002, http://www.physics.ucc.ie/fpetersweb/FrankWeb/courses/PY3108/Labs/PD_Info.pdf, accessed on December 2013.

17. Kingman, R., S. C. Rowland and S. Popescu, "An experimental observation of Faraday's law of induction", *American Journal of Physics*, Vol. 70, No. 6, pp.

595–598, 2002.

18. COMSOL, *Voltage Induced in a Coil by Moving Magnet*, 2012, http://www.comsol.com/model/voltage-induced-in-a-coil-by-moving-magnet-14163, accessed on August 2013.

19. Collins, S. H., and A. D. Kuo, "Dynamic arm swinging in human walking", *Proceedings of the Royal Society B*, Vol. 276, pp. 3679–3688, 2009.

20. OriginLab, *Linear and Polynomial Fitting*, http://www.originlab.com/index.aspx?go=Products/Origin/DataAnalysis/CurveFitting/LinearAndPolynomialFitting, accessed on April 2014.